A&A 597, A53 (2017)
DOI: 10.1051/0004-6361/201629180

Astronomy & Astrophysics

The ALMA-PILS survey: First detections of ethylene oxide, acetone and propanal toward the low-mass protostar IRAS 16293-2422

J. M. Lykke[1], A. Coutens[2], J. K. Jørgensen[1], M. H. D. van der Wiel[1], R. T. Garrod[3], H. S. P. Müller[4], P. Bjerkeli[1,5], T. L. Bourke[6], H. Calcutt[1], M. N. Drozdovskaya[7], C. Favre[8,9], E. C. Fayolle[10], S. K. Jacobsen[1], K. I. Öberg[10], M. V. Persson[7], E. F. van Dishoeck[7,11], and S. F. Wampfler[12]

[1] Centre for Star and Planet Formation, Niels Bohr Institute & Natural History Museum of Denmark, University of Copenhagen, Øster Voldgade 5–7, 1350 Copenhagen K., Denmark
e-mail: `juliemarialykke@gmail.com`
[2] Department of Physics and Astronomy, University College London, Gower St., London, WC1E 6BT, UK
[3] Departments of Chemistry and Astronomy, University of Virginia, Charlottesville, VA 22904, USA
[4] I. Physikalisches Institut, Universität zu Köln, Zülpicher Str. 77, 50937 Köln, Germany
[5] Department of Earth and Space Sciences, Chalmers University of Technology, Onsala Space Observatory, 439 92 Onsala, Sweden
[6] SKA Organization, Jodrell Bank Observatory, Lower Withington, Macclesfield, Cheshire SK11 9DL, UK
[7] Leiden Observatory, Leiden University, PO Box 9513, 2300 RA Leiden, The Netherlands
[8] Université Grenoble Alpes, IPAG, 38000 Grenoble, France
[9] CNRS, IPAG, 38000 Grenoble, France
[10] Harvard-Smithsonian Center for Astrophysics, 60 Garden Street, Cambridge, MA 02138, USA
[11] Max-Planck Institut für Extraterrestrische Physik (MPE), Giessenbachstr. 1, 85748 Garching, Germany
[12] Center for Space and Habitability (CSH), University of Bern, Sidlerstrasse 5, 3012 Bern, Switzerland

Received 24 June 2016 / Accepted 20 October 2016

ABSTRACT

Context. One of the open questions in astrochemistry is how complex organic and prebiotic molecules are formed. The unsurpassed sensitivity of the Atacama Large Millimeter/submillimeter Array (ALMA) takes the quest for discovering molecules in the warm and dense gas surrounding young stars to the next level.

Aims. Our aim is to start the process of compiling an inventory of oxygen-bearing complex organic molecules toward the solar-type Class 0 protostellar binary IRAS 16293-2422 from an unbiased spectral survey with ALMA, Protostellar Interferometric Line Survey (PILS). Here we focus on the new detections of ethylene oxide (c-C_2H_4O), acetone (CH_3COCH_3), and propanal (C_2H_5CHO).

Methods. With ALMA, we surveyed the spectral range from 329 to 363 GHz at 0.5″ (60 AU diameter) resolution. Using a simple model for the molecular emission in local thermodynamical equilibrium, the excitation temperatures and column densities of each species were constrained.

Results. We successfully detect propanal (44 lines), ethylene oxide (20 lines) and acetone (186 lines) toward one component of the protostellar binary, IRAS 16293B. The high resolution maps demonstrate that the emission for all investigated species originates from the compact central region close to the protostar. This, along with a derived common excitation temperature of $T_{\rm ex} \approx 125$ K, is consistent with a coexistence of these molecules in the same gas.

Conclusions. The observations mark the first detections of acetone, propanal and ethylene oxide toward a low-mass protostar. The relative abundance ratios of the two sets of isomers, a CH_3COCH_3/C_2H_5CHO ratio of 8 and a CH_3CHO/c-C_2H_4O ratio of 12, are comparable to previous observations toward high-mass protostars. The majority of observed abundance ratios from these results as well as those measured toward high-mass protostars are up to an order of magnitude above the predictions from chemical models. This may reflect either missing reactions or uncertain rates in the chemical networks. The physical conditions, such as temperatures or densities, used in the models, may not be applicable to solar-type protostars either.

Key words. astrochemistry – ISM: molecules – ISM: abundances – ISM: individual object: IRAS 16293-2422
line: identification – astrobiology

1. Introduction

An important task of modern-day astrochemistry is to understand how complex organics and possible pre-biotic molecules form near young stars. The high sensitivity and angular and spectral resolution of the Atacama Large Millimeter/submillimeter Array (ALMA) enables detection of molecular species with faint emission lines in otherwise confused regions. The capabilities of ALMA were demonstrated early on by the first detection of the prebiotic molecule glycolaldehyde toward the low-mass protostar, IRAS 16293-2422 (Jørgensen et al. 2012). This detection illustrates the potential for imaging emission from the simplest building blocks for biologically relevant molecules during the earliest stages of the Solar System on the scales where protoplanetary disks emerge, and for understanding how these molecules are formed and in what abundances. This paper presents the first detections of three such species, ethylene oxide (c-C_2H_4O), propanal (C_2H_5CHO) and acetone (CH_3COCH_3)

toward IRAS 16293-2422 from an unbiased spectral survey with ALMA (Protostellar Interferometric Line Survey or PILS; Jørgensen et al. 2016).

Traditionally, detections of complex organic molecules have mostly been associated with the hot cores around high-mass protostars toward the warm and dense central regions around such luminous sources where the molecules sublimate from the icy mantles of dust grains. Some low-mass protostars show similar characteristics on small scales; the so-called *hot corinos* (van Dishoeck & Blake 1998; Bottinelli et al. 2004; Ceccarelli 2004). A prime example of this is IRAS 16293-2422 (IRAS 16293 hereafter), a protostellar Class 0 binary system, located at a distance of 120 pc (Loinard et al. 2008). IRAS 16293 is perhaps the best low-mass protostellar testbed for astrochemical studies (see, e.g., Blake et al. 1994; van Dishoeck et al. 1995; Ceccarelli et al. 2000; Schöier et al. 2002). It has the brightest lines by far of all well-studied low-mass protostars and shows detections of a wealth of complex organic molecules (Cazaux et al. 2003; Caux et al. 2011). These complex organics arise in the dense gas around each of its two binary components that each show distinct chemical signatures in the warm gas on small scales resolved by (sub)millimeter wavelength aperture synthesis observations (Bottinelli et al. 2004; Kuan et al. 2004; Bisschop et al. 2008; Jørgensen et al. 2011).

To understand how these complex organic molecules form, combinations of systematic studies establishing large inventories of similar organic molecules are needed. For this purpose, structural isomers are particularly interesting since they usually share some formation and destruction pathways. The relative abundance of two such isomers may therefore provide important constraints on astrochemical models. Examples of such interesting isotope pairs are ethylene oxide and acetaldehyde as well as acetone and propanal. Ethylene oxide was first detected toward the galactic center source Sagittarius B2(N) (Sgr B2(N)) by Dickens et al. (1997; confirmed by Belloche et al. 2013), and has since been observed in several massive star-forming regions (Nummelin et al. 1998; Ikeda et al. 2001) but so far not toward any low-mass protostar. Acetone (CH_3COCH_3), also called propanone, was the first molecule with ten atoms to be observed in the ISM. The molecule was first detected in the hot molecular core Sgr B2 (Combes et al. 1987; Snyder et al. 2002) and later in the Orion-KL star-forming region (Friedel et al. 2005; Friedel & Snyder 2008; Peng et al. 2013). It was also detected toward other massive star-forming regions (Isokoski et al. 2013) as well as toward an intermediate-mass protostar (Fuente et al. 2014). Several lines of the SMA survey of IRAS 16293 were also assigned to acetone by Jørgensen et al. (2011), but it has never been properly identified in this source. More recently, it was found in material from the comet 67P/Churyumov-Gerasimenko by the COmetary Sampling And Composition (COSAC) experiment on Rosetta's lander Philae (Goesmann et al. 2015). Propanal (C_2H_5CHO) has previously been detected in Sgr B2(N) by Hollis et al. (2004), where it coexists with propynal and propenal. It was also detected towards two Galactic center molecular clouds by Requena-Torres et al. (2008). Like acetone, propanal was found to be present in the comet 67P/Churyumov-Gerasimenko (Goesmann et al. 2015).

This paper presents detections of ethylene oxide, acetone and propanal toward IRAS 16293 utilising a large ALMA survey at (sub)millimeter wavelength. These are all first time detections in IRAS 16293 and in low-mass protostars in general. In Sect. 2, we briefly describe the observations. The identification and analysis of the data are presented in Sect. 3. Finally, we discuss the results in Sect. 4 and conclude in Sect. 5.

2. Observations

IRAS 16293 was observed as part of the PILS program (PI: Jes K. Jørgensen): the survey consists of an unbiased spectral survey covering a significant part of ALMA's Band 7 (wavelengths of approximately 0.8 mm) as well as selected windows in ALMA's Bands 3 (at approximately 100 GHz; 3 mm) and 6 (at approximately 230 GHz; 1.3 mm). In this paper we only utilise data from the Band 7 part of the survey (project-id: 2013.1.00278.S). An observing log, a description of the data reduction and a first overview of the data are presented in Jørgensen et al. (2016) and here we only summarize a number of the key features of the Band 7 observations.

The Band 7 part of the survey covers the frequency range from 329.15 GHz to 362.90 GHz in full. Data were obtained from both the array of 12 m dishes (typically 35–40 antenna in the array at the time of observations) and the Atacama Compact Array (ACA), or "Morita Array", of 7 m dishes (typically 9–10 antenna in use). The pointing center was in both cases set to be a location in-between the two components of the binary system at $\alpha_{J2000} = 16^h32^m22.72^s$; $\delta_{J2000} = -24°28'34''.3$. In total 18 spectral settings were observed: each setting covers a bandwidth of 1875 MHz (over four different spectral windows of 468.75 MHz wide). To limit the data-rate, the data were downsampled by a factor two to the native spectral resolution of the ALMA correlator, resulting in a spectral resolution of 0.244 MHz ($\approx$0.2 km s^{-1}) over 1920 channels for each spectral window. Each setting was observed with approximately 13 min integration on source (execution blocks of approximately 40 min including calibrations) for the 12 m array and double that for the ACA.

The data for each setting were calibrated and a first imaging of the continuum was performed. Thereafter, a phase-only self-calibration was performed on the continuum images and applied to the full datacubes before combining the 12 m array and ACA data and performing the final cleaning and imaging. The resulting spectral line datacubes have an root mean square (RMS) noise for the combined datasets of approximately 6–8 mJy $beam^{-1}$ $channel^{-1}$, which translates into a uniform sensitivity better than 5 mJy $beam^{-1}$ km s^{-1} with beam sizes ranging from $\approx$0.4–0.7″ depending on the exact configuration at the date of observation. The data used in this paper were produced with a circular restoring beam of 0.5″ to facilitate the analysis across the different spectral windows. The conversion from Rayleigh-Jeans temperature T_b[K] to flux density S_ν[Jy/beam] follows the standard formulation and T_b/S_ν ranges from 37.2 to 45.2 K Jy^{-1} depending on the frequency. The resulting image cubes are strongly line-confused toward the locations of the two primary protostars. A subtraction of the continuum was therefore done statistically for each spectral window (for continuum maps and more details see Jørgensen et al. 2016). The continuum baseline for each window is found to be robust to within twice the RMS in each channel.

3. Analysis and results

Interferometric emission maps of two representive lines each for propanal, acetone, ethylene oxide, and acetaldehyde are shown in Fig. 1. The maps show emission toward both protostellar sources. Generally the lines toward IRAS 16293A are approximately a factor five broader than toward IRAS 16293B (e.g., Bottinelli et al. 2004; Jørgensen et al. 2011), which makes identification of individual species challenging. Consequently IRAS 16293B is therefore better for separation of blended lines

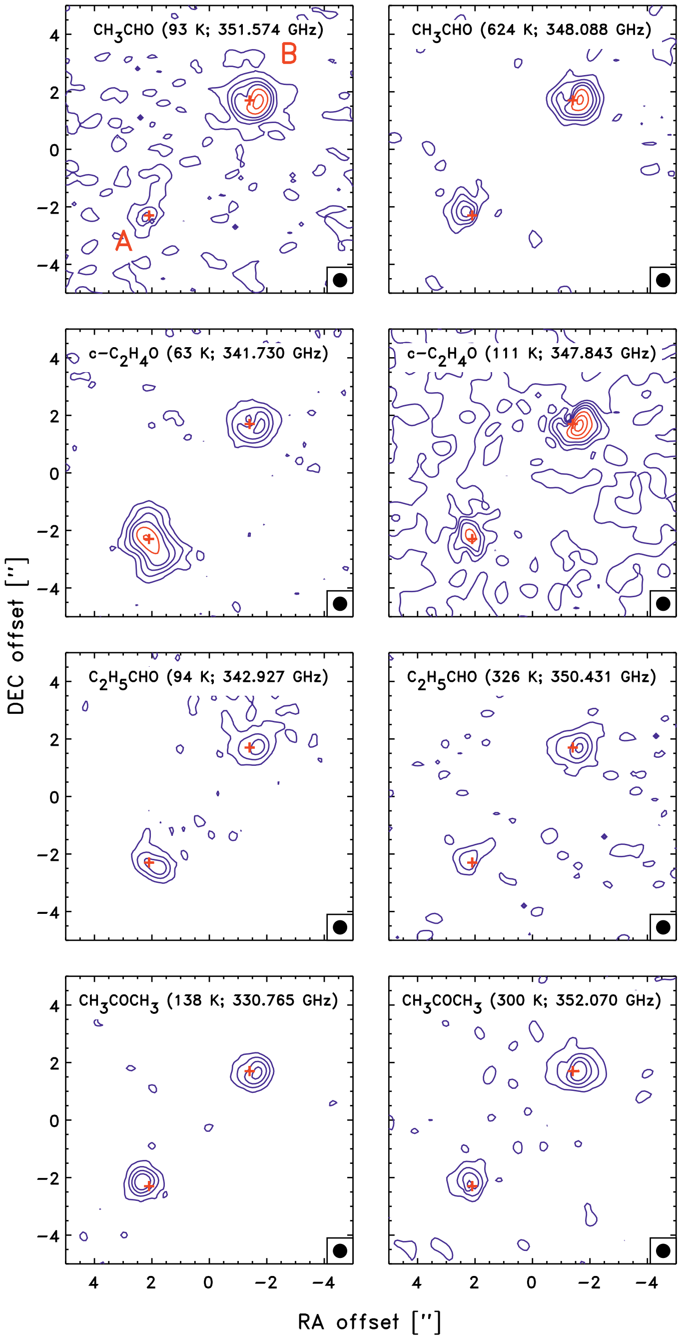

Fig. 1. Integrated intensity maps of the line emission for acetaldehyde, ethylene oxide, acetone, and propanal. *Left and right columns* show maps for transitions with lower and higher $E_{\rm up}$, respectively. The locations of IRAS 16293A (southeast) and IRAS 16293B (northwest) are marked by the red plus-signs. The blue contours represent 4, 8, 12 and 16σ while the red contours show 24, 30, 36σ, where σ is 5 mJy beam^{-1} km s^{-1} for the integrated intensity. A representative beam of 0.5″ is shown in the lower right-hand corner of each panel.

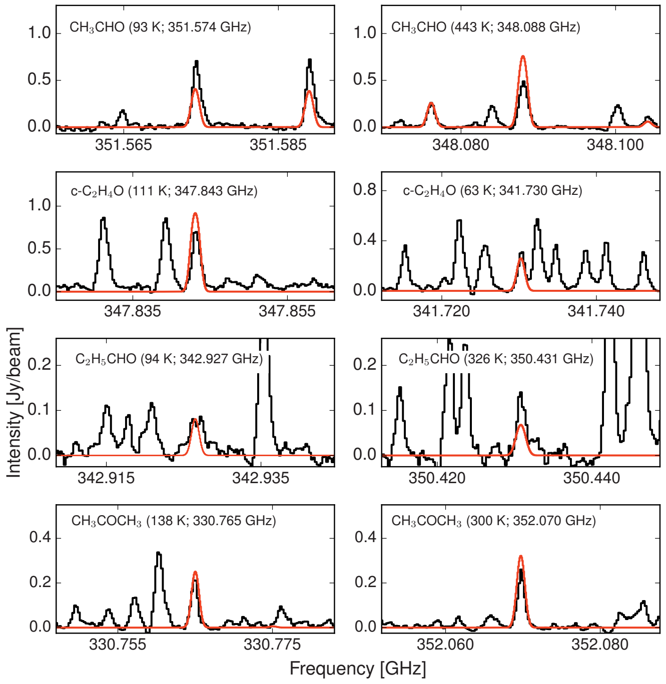

Fig. 2. Observed and synthetic spectra of the representative transitions shown in Fig. 1. The observed spectra are extracted at a position (−0.45″; −0.30″) southwest of the continuum peak of IRAS 16293B.

and identification of new species and in this paper we focus on that source. A comparison of the maps for the different molecules shows that the emission is marginally resolved toward IRAS 16293B, consistent with a deconvolved extent of ≈0.5″ toward the location of the protostar for all species. We can therefore assume that these particular molecules coexist and trace the same gas. Extracting a spectrum from the pixel located on the peak position will give the highest emission signal, but since the continuum is optically thick and very bright there are also very prominent absorption lines in the spectrum. To reduce the influence of absorption while still retaining as much intensity in the emission lines as possible, we extracted a spectrum from a position at $\alpha_{\rm J2000} = 16^{\rm h}32^{\rm m}22.58^{\rm s}$; $\delta_{\rm J2000} = -24^\circ28'32\overset{''}{.}8$, corresponding to an offset of (−0.45″; −0.30″) in the southwestern direction relative to the continuum peak of IRAS 16293B. This spectrum, corrected for the LSR velocity ($V_{\rm LSR} = 2.7$ km s^{-1}), is used throughout this paper. Figure 2 shows the observed spectra for each of the transitions from Fig. 1.

The heavy blending of emission lines at the sensitivity of ALMA complicates the identification and analysis of individual molecular species. For this purpose we therefore calculate synthetic spectra for our target molecules and their physical parameters are derived by fitting synthetic spectra to the data. For the purpose of excluding blended lines from the analysis, we create a reference model containing the synthetic spectrum of emission lines of previously detected complex organic molecules that are expected to be present in the warm gas toward the two sources (Bisschop et al. 2008; Jørgensen et al. 2011, 2012, 2016; Coutens et al. 2016). Superimposing the reference model spectrum onto the observed spectrum reveals if a line of interest is blended with any of these species. For our analysis we exclude lines that are severely blended, that is, where the peaks of the emission lines overlap. In addition, we have also checked the lines of interest against other species in the CDMS[1] and JPL[2] databases (Müller et al. 2001, 2005; Pickett et al. 1998) with the CASSIS[3] software and do not find any clear overlap with any other potential interstellar species.

The synthetic spectra are computed following the approach described in Goldsmith & Langer (1999). We assume that the

---

[1] `http://www.astro.uni-koeln.de/cdms`
[2] `http://spec.jpl.nasa.gov/`
[3] `http://cassis.irap.omp.eu/`

molecular excitation obeys local thermodynamic equilibrium (LTE), which is reasonable at the densities and scales of the ALMA observations toward IRAS 16293B (Jørgensen et al. 2016), and calculate a synthetic spectrum of all transitions from a molecule given a line width, column density, rotational temperature, and source size, assuming Gaussian line profiles. The spectroscopic data for propanal (Butcher & Wilson Jr. 1964; Hardy et al. 1982; Demaison et al. 1987) and ethylene oxide (Cunningham Jr. et al. 1951; Creswell & Schwendemann 1974; Hirose 1974; Pan et al. 1998; Medcraft et al. 2012) are available from the CDMS database, while the spectroscopic data for acetone (Groner et al. 2002) and acetaldehyde (Kleiner et al. 1996) are available from the JPL database.

For the analysis we started by identifying the brightest potential lines of each of the relevant species adopting a full width half maximum (FWHM) line width and the source size remained fixed at 1.0 km s^{-1} and 0.5″, respectively. We then generated a synthetic spectrum by adjusting the temperature and column density ($N_{\rm tot}$) until a good fit for those lines was obtained. From this a priori spectrum, we identified approximately ten reasonably non-blended and optically thin ($\tau \leq 0.1$) lines for each species, which we use to minimize the reduced chi-squared statistic:

$$\chi^2_{\rm red.} = \frac{1}{N}\sum_{i=1}^{N}\left(\frac{\left(I_{{\rm obs},i} - I_{{\rm syn},i}\right)}{\sigma_i}\right)^2, \quad (1)$$

where $I_{\rm obs}$ and $I_{\rm syn}$ are the intensities of the observed and synthetic emission lines, respectively, N is the number of lines analyzed and σ the RMS error. In the analysis, we varied the column density from 1.0×10^{14} cm^{-2} – 1.0×10^{18} cm^{-2} with small increments and the temperature from 100 K–400 K with increments of 25 K, generating a new synthetic spectrum at each increment to evaluate against the observed spectrum at the locations of the chosen lines. Since the emission lines are blended, the reduced χ^2 is only calculated for the average value of the channels at the very peak of the lines (corresponding to the predicted frequency of the peak ±0.25 MHz), instead of over the entire Gaussian bell curve.

From the reduced χ^2 analysis, acetaldehyde and ethylene oxide show the best fit at $T_{\rm ex} \approx 125$ K, while it is difficult to constrain the excitation temperature for propanal and acetone. Our analysis shows that the column densities do not vary greatly with temperature for all species, except for acetone, where a $T_{\rm ex} = 400$ K results in a column density a factor of ten higher than for $T_{\rm ex} = 100$ K. A comparison between the synthetic and observed spectrum for acetone reveals that an excitation temperature of approximately 200 K could still be in agreement with the observations, but that a $T_{\rm ex}$ of 300 K overproduces some of the lines. Since it appears that the molecules are spatially coexisting and trace the same gas, we therefore assume $T_{\rm ex} = 125$ K for all molecules. The resulting column densities are summarized in Table 1 and the relative abundance ratios of the different isomers are listed in Table 2. The uncertainties of $T_{\rm ex}$ and $N_{\rm tot}$ are dominated by the assumptions that go into the analysis, that is, LTE and Gaussian line profiles, instead of the statistical error. Therefore, the uncertainties are estimated to ~50% and 25 K on the column density and the emission temperature, respectively.

Figures A.1–A.3 show the synthetic spectra of ethylene oxide, propanal, and acetone, respectively, as well as the reference model superimposed on the observed spectrum for all lines where the synthetic spectrum predicts a peak line intensity equal to or above twice the RMS noise of the spectrum. The lines are sorted into descending intensity. We check each line in the synthetic spectra against the observed spectrum for each molecule, and the majority of them provide a reasonable match, within the estimated uncertainty. We claim a detection for lines i) that are reasonably well separated from other species in the reference model and ii) where the integrated line strength over FWHM is larger than three times the statistical uncertainty ($\sqrt{n_{\rm chan}} \times$ RMS) of the line and iii) where there is a reasonably good fit between the synthetic and the observed spectrum. Table B.1 lists the spectroscopic catalog values, the integrated intensity over the FWHM for the observed spectrum, and the detection level for the detected lines of ethylene oxide, propanal, and acetone. The transitions are listed with increasing frequency and it should be noted that many of the detected lines are a blend of several internal rotation components.

Table 1. Best fit column densities.

Molecule		$N_{\rm tot}$ [cm^{-2}]
Acetone	CH_3COCH_3	1.7×10^{16}
Propanal	C_2H_5CHO	2.2×10^{15}
Acetaldehyde	CH_3CHO	7.0×10^{16}
Ethylene oxide	c-C_2H_4O	6.1×10^{15}

Notes. The results are derived assuming $\theta_{\rm source} = 0.5''$, $T_{\rm ex} = 125$ K and $FWHM = 1.0$ km s^{-1}. The column density of propanal was corrected by a factor of 1.489 to take into account the vibrational and conformational contribution at $T = 125$ K.

For ethylene oxide, propanal, and acetone, we detected 20, 44, and 186 lines, respectively. Some of the acetone lines predicted by the models appear to be either slightly shifted or missing. In some cases, this can be explained by the presence of absorption at the same frequency as the predicted lines, but in most cases these lines correspond to transitions with both high $K_{\rm a}$ and low $K_{\rm c}$ quantum numbers (see Table C.1). None of the missing or shifted lines with high $K_{\rm a}$ and low $K_{\rm c}$ numbers were used for the determination of the spectroscopic parameters. It was admitted by Groner et al. (2002) that these lines do not fit very well. It could be due to perturbations from interactions between the (high $K_{\rm a}$, low $K_{\rm c}$) levels and the levels from the lowest torsional excited states (Groner et al. 2002).

We also search for vinyl alcohol (Saito 1976), another isomer of acetaldehyde and ethylene oxide, but no detection can be claimed so far. With a conservative upper limit of 2×10^{15} cm^{-2} for the syn form (the lowest energy form of vinyl alcohol), this isomer is less abundant than acetaldehyde and ethylene oxide, similarly to what was found in Sgr B2 by Belloche et al. (2013).

4. Discussion

As described in the introduction, the relative abundances of the different isomers are important constraints on chemical models and provide insight into the formation of the complex species. Table 2 lists the different abundance ratios and Fig. 3 gives a schematic overview of the entries from the table. A number of different formation pathways have been proposed for the studied species.

For acetone, the ion-molecule radiative association reaction

$$CH_3^+ + CH_3CHO \rightarrow (CH_3)_2CHO^+ + h\nu, \quad (2)$$

followed by

$$(CH_3)_2CHO^+ + e^- \rightarrow CH_3COCH_3 + H, \quad (3)$$

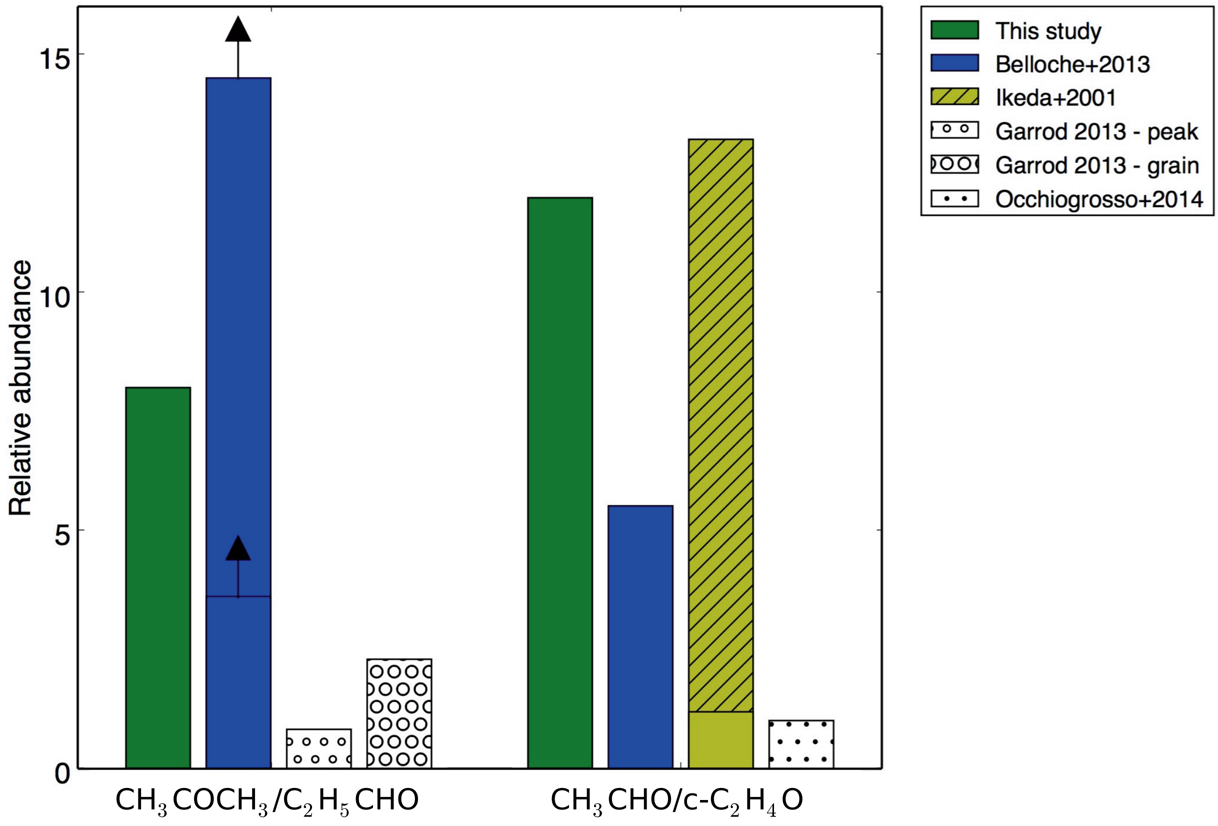

Fig. 3. Bar plot of the relative abundances of CH_3COCH_3/ C_2H_5CHO and $CH_3CHO/c\text{-}C_2H_4O$ from Table 1. The observations are indicated by color bars, while the chemical predictions are shown by white bars with different circle sizes. The two lower limits derived by Belloche et al. (2013) for CH_3COCH_3/C_2H_5CHO are illustrated by upward arrows. The range of CH_3CHO/ $c\text{-}C_2H_4O$ ratios determined in ten sources by Ikeda et al. (2001) is indicated by the hatched area. For the CH_3CHO/ $c\text{-}C_2H_4O$ ratio from Belloche et al. (2013), we used the average value of the column densities of the rotational and first torsionally ($v_t = 1$) excited states of acetaldehyde.

Table 2. Relative abundances in different sources.

Source	CH_3COCH_3/C_2H_5CHO	$CH_3CHO/c\text{-}C_2H_4O$	References
IRAS 16293-2422	8	12	this study
Sgr B2(N)	$\geq$3.6–14.5[a]	3.7–7.4[b]	Belloche et al. (2013)
Survey of massive SF regions	–	1.2–13.2	Ikeda et al. (2001)
Chemical model: peak gas-phase	0.22: 0.83: 0.07[c]	–	Garrod (2013)
Chemical model: peak grain-surface	0.37: 2.3: 0.39[c]	–	Garrod (2013)
Chemical model of hot cores	–	1[d]	Occhiogrosso et al. (2014)

Notes. [a] Range reflects span for rotational states in the $V_{\rm off} = 0$ km s^{-1} and the $V_{\rm off} = 10$ km s^{-1} components of Sgr B2(N). Propanal is not detected, therefore the upper limit is used after correction for a similar beam filling factor. [b] Range reflects span for the rotational and first torsionally ($v_t = 1$) excited states of acetaldehyde in the $V_{\rm off} = -1$ km s^{-1} component of Sgr B2(N). [c] Chemical model of hot cores for a slow, medium, and fast model, respectively. [d] The MONACO code (at 200 K and 1.2×10^6 yr).

proposed by Combes et al. (1987) has been shown not to be efficient enough to produce the observed values (Herbst et al. 1990). In the model presented by Garrod et al. (2008), acetone is formed on grains by the addition of CH_3 to CH_3CO.

Hollis et al. (2004) proposed the formation of propanal to occur through simple successive hydrogenation:

$$HC_2CHO + 2H \rightarrow CH_2CHCHO + 2H \rightarrow C_2H_5CHO. \quad (4)$$

However, Garrod (2013) proposed a different formation route through the addition of HCO and C_2H_5 radicals on grains. Garrod (2013) found the formation to be most rapid at 30 K, when sublimation of grain-surface methane (CH_4) is most efficient.

Laboratory experiments were conducted by Bennett et al. (2005a,b) to study the synthesis of acetaldehyde, ethylene oxide, and vinyl alcohol in interstellar and cometary ices after irradiation with energetic electrons. Acetaldehyde appeared to be formed in both CO–CH_4 and CO_2–C_2H_4 ice mixtures, while ethylene oxide and vinyl alcohol are only detected in CO_2–C_2H_4 ice mixtures (Bennett et al. 2005a,b). While CO, CO_2, and CH_4 have been observed in interstellar ices, C_2H_4 is formed as a secondary product by charged particle irradiation and photolysis of CH_4 ices and it is therefore likely only present in small concentrations (Bennett et al. 2005b) although it may be formed through gas-phase mechanisms under cold, dense conditions. Thus, assuming the relative production rates of acetaldehyde, ethylene oxide and vinyl alcohol are similar, the fractional abundance of acetaldehyde is expected to be higher than that of ethylene oxide and vinyl alcohol (Bennett et al. 2005b).

4.1. Propanal and acetone

We have compared our results to predictions from the three-phase (mantle/surface/gas) astrochemical kinetics model, MAGICKAL (Model for Astrophysical Gas and Ice Chemical Kinetics And Layering), as presented in Garrod (2013). By applying a chemical network to hot-core conditions, the model follows the physico-chemical evolution of a parcel of material from the core from the free-fall collapse of the cloud to the subsequent warm-up phase of the dense core from 8 to 400 K (Garrod 2013). MAGICKAL employs a (modified) rate-equation approach to solve the coupled ice mantle, ice-surface, and gas-phase chemistry allowing radicals on the grains to meet via thermal diffusion at intermediate temperatures and form more complex molecules prior to the complete sublimation of the dust-grain ice at higher temperatures. Garrod (2013) uses three different warm-up models: *fast*, *medium* and *slow*. Here we compare our results to all three models, but note that the fast warm-up model should, in principle, be the best match to the observations because the time for this model to reach 200 K is 5×10^4 yr which is comparable to the dynamical age of $\sim$1–3×10^4 yr for IRAS 16293 as derived by Schöier et al. (2002).

Garrod (2013) finds relative peak gas-phase abundances of CH_3COCH_3/C_2H_5CHO of 0.22, 0.83, and 0.07 for the fast, medium and slow model, respectively. All three models predict a higher abundance of propanal compared to acetone, which is the opposite trend of our ratio of eight. Also, the upper limit toward Sgr B2(N) reported by Belloche et al. (2013) translates into a lower limit for CH_3COCH_3/C_2H_5CHO of 3.6, which is consistent with our findings. One explanation may be that the model of Garrod (2013) uses a relatively low binding energy for acetone (3500 K), producing a desorption temperature of approximately 70 K. As discussed by Garrod et al. (2008), this low-temperature desorption results in rapid destruction of acetone in the gas-phase. Our observational fit to the excitation temperature of 125 K suggests that acetone is more likely desorbed from grains at the higher temperatures more commonly associated with complex organics, which would allow the majority of grain-surface formed acetone to survive for a significant period in the gas phase.

If we compare the peak *grain-surface* abundances of acetone and propanal produced in the Garrod (2013) chemical model which would be more representative of this situation, ratios of 0.37, 2.3, and 0.39 are obtained, respectively. The quantities of acetone and propanal produced on grains in the model are, in the case of the intermediate warm-up timescale, only a factor of a few below the observed ratio. However, it should be borne in mind that the efficient production of acetone depends, in this model, on the rate at which the CH_3CO radical may be produced on the grains. This may be achieved either through direct photodissociation of CH_3CHO or by the abstraction of a H-atom from this molecule by OH or NH_2. The rates of each of these processes are not well defined by experiment, and these uncertainties could easily induce a variation in acetone production of a few factors. It is also likely that the physical conditions, which in the Garrod (2013) model are generic, representative hot-core conditions, may not be accurate for the specific case of IRAS 16293.

4.2. Ethylene oxide and acetaldehyde

Ikeda et al. (2001) searched for acetaldehyde and ethylene oxide in several massive star-forming regions. They detect both molecules in ten sources and find $CH_3CHO/c\text{-}C_2H_4O$ spanning a range from 1.2 in Sgr B2(N) to 13.2 in W51e1/e2. Belloche et al. (2013) also observed these molecules towards Sgr B2(N) and found a slightly higher value than Ikeda et al. (2001) of 3.7–7.4. It thus seems that our observed value of 12 in a low-mass YSO is toward the high end of the range observed in these high-mass regions, but that source-to-source variations may be larger than between the different groups of sources.

Occhiogrosso et al. (2014) used a two-stage (grain/gas) model, MONACO, to predict the gaseous acetaldehyde and ethylene oxide abundances during the cooling-down and subsequent warm-up phase of a hot core. At 200 K and 1.2×10^6 yr, the fractional abundance of ethylene oxide and acetaldehyde with respect to total H is 2×10^{-9} for both molecules, which means that the relative abundance between the two species is unity. As previously mentioned, based on their laboratory experiments, Bennett et al. (2005a,b) expect the relative abundance of $CH_3CHO/c\text{-}C_2H_4O$ to be larger than unity. Again, it seems that there are some variations in the observed acetaldehyde-to-ethylene oxide ratios, and that the model results of Occhiogrosso et al. (2014) best reproduce the lower end in that range, while our measurements are at the opposite end, more than an order of magnitude above. Nevertheless, given the variations seen in the models for acetone and propanal, whether the specific physical structures of the sources can be part of the explanation remains to be explored.

5. Conclusion

We have carried out the first investigation of the oxygen bearing species in the ALMA PILS survey of the protostellar binary system IRAS 16293. Our main findings are summarized as follows:

1. We have detected the molecules ethylene oxide ($c\text{-}C_2H_4O$), acetone (CH_3COCH_3), and propanal (C_2H_5CHO) for the first time toward a solar-type protostar. We have verified that the emission of these species, along with acetaldehyde (CH_3CHO), originates from the compact central region of the protostar, which confirms our assumption that these molecules spatially coexist. We determined a common excitation temperature, $T_{\rm ex} \approx 125$ K for all four molecules and use this to determine column densities for each species.
2. Compared to previous observations, our results for the relative abundance ratio of CH_3COCH_3/C_2H_5CHO are consistent with the lower limit found by Belloche et al. (2013) of SgrB2(N). The ratio for $CH_3CHO/c\text{-}C_2H_4O$ is comparable to the largest value in the span of observed values of high-mass sources from Ikeda et al. (2001) (variation between the sources in that sample of approximately an order of magnitude). This suggests that the chemistry in the most central part of IRAS 16293 (the hot corino region) is not significantly different from those of the high-mass hot cores, but that there may still be measurable source-to-source variations.
3. Contrary to our result, the models in Garrod (2013) predict propanal to be more abundant than acetone, except for the peak grain-surface abundances in the medium warm-up model, where the prediction is only few factors different from our result. Occhiogrosso et al. (2014) find the ratio of $CH_3CHO/c\text{-}C_2H_4O$ to be unity which is consistent with the

lowest observed value of a high-mass star forming region (Ikeda et al. 2001). All of the models investigated here return low relative abundances compared to our results, but they are however in reasonable agreement with the lowest value in the ranges reported by Ikeda et al. (2001) and Belloche et al. (2013).

The results from this paper imply that although the chemical models can reproduce the observations for some high-mass protostars reasonably well, they need to be modified to reflect the observed range of values for high-mass sources as well as our low-mass source. As discussed, the models would improve with better-defined reaction rates while including more species in the chemical networks could also improve model predictions. More observations, in particular toward low-mass sources, are needed for comparison with models to further constrain the formation pathways.

The detections also demonstrate the great potential of spectral surveys such as PILS for identifying new species that have so far gone undetected toward solar-type stars. New detections of complex organic molecules and the determination of their relative abundances for the first time in a solar-type protostar is important because it substantiates the chemical complexity of IRAS 16293 and can be used to constrain astrochemical models. The relative abundances reveal information of the formation pathway of the molecules and enable comparisons with models and laboratory experiments. In addition, the comparison of the ratios found in high-mass sources and low-mass protostars is vital to understanding the environmental effects on the formation of different molecular species.

Acknowledgements. This research was made possible through a Lundbeck Foundation Group Leader Fellowship as well as the European Research Council (ERC) under the European Union Horizon 2020 research and innovation programme (grant agreement No. 646908) through ERC Consolidator Grant "S4F" to J.K.J. Research at Centre for Star and Planet Formation is funded by the Danish National Research Foundation. The work of A.C. was funded by the STFC grant ST/M001334/1. A.C. thanks the COST action CM1401 Our Astrochemical History for additional financial support. R.T.G. acknowledges the support of the NASA APRA program, though grant NNX15AG07G. Astrochemistry in Leiden is supported by the European Union A-ERC grant 291141 CHEMPLAN, by the Netherlands Research School for Astronomy (NOVA), by a Royal Netherlands Academy of Arts and Sciences (KNAW) professor prize. The research leading to these results has received funding from the European Commission Seventh Framework Programme (FP/2007-2013) under grant agreement No. 283393 (RadioNet3). This paper makes use of the following ALMA data: ADS/JAO.ALMA#2013.1.00278.S. ALMA is a partnership of ESO (representing its member states), NSF (USA) and NINS (Japan), together with NRC (Canada) and NSC and ASIAA (Taiwan), in cooperation with the Republic of Chile. The Joint ALMA Observatory is operated by ESO, AUI/NRAO and NAOJ.

References

Belloche, A., Müller, H. S. P., Menten, K. M., Schilke, P., & Comito, C. 2013, A&A, 559, A47
Bennett, C. J., Jamieson, C. S., Osamura, Y., & Kaiser, R. I. 2005a, ApJ, 624, 1097
Bennett, C. J., Osamura, Y., Lebar, M. D., & Kaiser, R. I. 2005b, ApJ, 634, 698
Bisschop, S. E., Jørgensen, J. K., Bourke, T. L., Bottinelli, S., & van Dishoeck, E. F. 2008, A&A, 488, 959
Blake, G. A., van Dishoeck, E. F., Jansen, D. J., Groesbeck, T. D., & Mundy, L. G. 1994, ApJ, 428, 680
Bottinelli, S., Ceccarelli, C., Neri, R., et al. 2004, ApJ, 617, L69
Butcher, S. S., & Wilson Jr., E. B. 1964, J. Chem. Phys., 40, 1671
Caux, E., Kahane, C., Castets, A., et al. 2011, A&A, 532, A23
Cazaux, S., Tielens, A. G. G. M., Ceccarelli, C., et al. 2003, ApJ, 593, L51
Ceccarelli, C. 2004, in Star Formation in the Interstellar Medium: in Honor of David Hollenbach, eds. D. Johnstone, F. C. Adams, D. N. C. Lin, D. A. Neufeld, & E. C. Ostriker, ASP Conf. Ser., 323, 195
Ceccarelli, C., Castets, A., Caux, E., et al. 2000, A&A, 355, 1129
Combes, F., Gerin, M., Wootten, A., et al. 1987, A&A, 180, L13
Coutens, A., Jørgensen, J. K., van der Wiel, M. H. D., et al. 2016, A&A, 590, L6
Creswell, R. A., & Schwendemann, R. H. 1974, Chem. Phys. Lett., 27, 521
Cunningham Jr., G. L., Boyd, A. W., Mayers, R. J., Gwinn, W. D., & Le Van, W. I. 1951, J. Chem. Phys., 19, 676
Demaison, J., Maes, H., van Eijck, B. P., Wlodarczak, G., & Lasne, M. C. 1987, J. Mol. Spectrosc., 125, 214
Dickens, J. E., Irvine, W. M., Ohishi, M., et al. 1997, ApJ, 489, 753
Friedel, D. N., & Snyder, L. E. 2008, ApJ, 672, 962
Friedel, D. N., Snyder, L. E., Remijan, A. J., & Turner, B. E. 2005, ApJ, 632, L95
Fuente, A., Cernicharo, J., Caselli, P., et al. 2014, A&A, 568, A65
Garrod, R. T. 2013, ApJ, 765, 60
Garrod, R. T., Weaver, S. L. W., & Herbst, E. 2008, ApJ, 682, 283
Goesmann, F., Rosenbauer, H., Bredehöft, J. H., et al. 2015, Science, 349, 020689
Goldsmith, P. F., & Langer, W. D. 1999, ApJ, 517, 209
Groner, P., Albert, S., Herbst, E., et al. 2002, ApJS, 142, 145
Hardy, J. A., Cox, A. P., Fliege, E., & Dreizler, H. 1982, Z. Naturforsch, 37, 1035
Herbst, E., Giles, K., & Smith, D. 1990, ApJ, 358, 468
Hirose, C. 1974, ApJ, 189, L145
Hollis, J. M., Jewell, P. R., Lovas, F. J., Remijan, A., & Møllendal, H. 2004, ApJ, 610, L21
Ikeda, M., Ohishi, M., Nummelin, A., et al. 2001, ApJ, 560, 792
Isokoski, K., Bottinelli, S., & van Dishoeck, E. F. 2013, A&A, 554, A100
Jørgensen, J. K., Bourke, T. L., Nguyen Luong, Q., & Takakuwa, S. 2011, A&A, 534, A100
Jørgensen, J. K., Favre, C., Bisschop, S. E., et al. 2012, ApJ, 757, L4
Jørgensen, J. K., van der Wiel, M. H. D., Coutens, A., et al. 2016, A&A, 595, A117
Kleiner, I., Lovas, F. J., & Godefroid, M. 1996, Phys. Chem. Ref. Data, 25, 1113
Kuan, Y., Huang, H., Charnley, S. B., et al. 2004, ApJ, 616, L27
Loinard, L., Torres, R. M., Mioduszewski, A. J., & Rodríguez, L. F. 2008, ApJ, 675, L29
Medcraft, C., Thompson, C. D., Robertson, E. G., Appadoo, D. R. T., & McNaughton, D. 2012, ApJ, 753, 18
Müller, H. S. P., Schlöder, F., Stutzki, J., & Winnewisser, G. 2005, J. Mol. Struct., 742, 215
Müller, H. S. P., Thorwirth, S., Roth, D. A., & Winnewisser, G. 2001, A&A, 370, L49
Nummelin, A., Dickens, J. E., Bergman, P., et al. 1998, A&A, 337, 275
Occhiogrosso, A., Vasyunin, A., Herbst, E., et al. 2014, A&A, 564, A123
Pan, J., Albert, S., Sastry, K. V. L. N., Herbst, E., & De Lucia, F. C. 1998, ApJ, 499, 517
Peng, T.-C., Despois, D., Brouillet, N., et al. 2013, A&A, 554, A78
Pickett, H. M., Poynter, I. R. L., Cohen, E. A., et al. 1998, J. Quant. Spectr. Rad. Transf., 60, 883
Requena-Torres, M. A., Martín-Pintado, J., Martín, S., & Morris, M. R. 2008, ApJ, 672, 352
Saito, S. 1976, Chem. Phys. Lett., 42, 399
Schöier, F. L., Jørgensen, J. K., van Dishoeck, E. F., & Blake, G. A. 2002, A&A, 390, 1001
Snyder, L. E., Lovas, F. J., Mehringer, D. M., et al. 2002, ApJ, 578, 245
van Dishoeck, E. F., & Blake, G. A. 1998, ARA&A, 36, 317
van Dishoeck, E. F., Blake, G. A., Jansen, D. J., & Groesbeck, T. D. 1995, ApJ, 447, 760

Appendix A: Observed and synthetic spectra

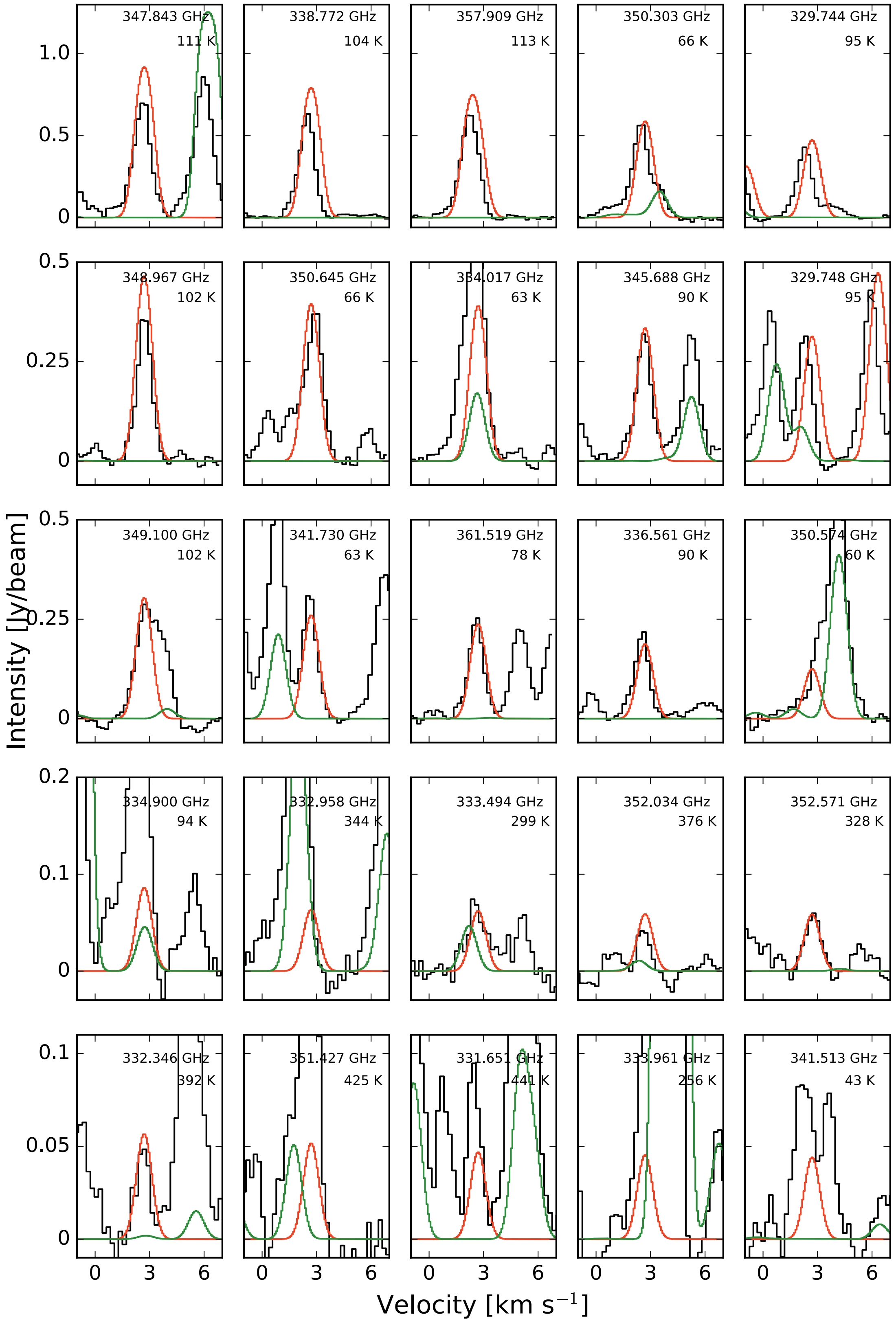

Fig. A.1. Ethylene oxide (c-C_2H_4O): synthetic spectrum in red and reference model in green superimposed onto observed spectrum.

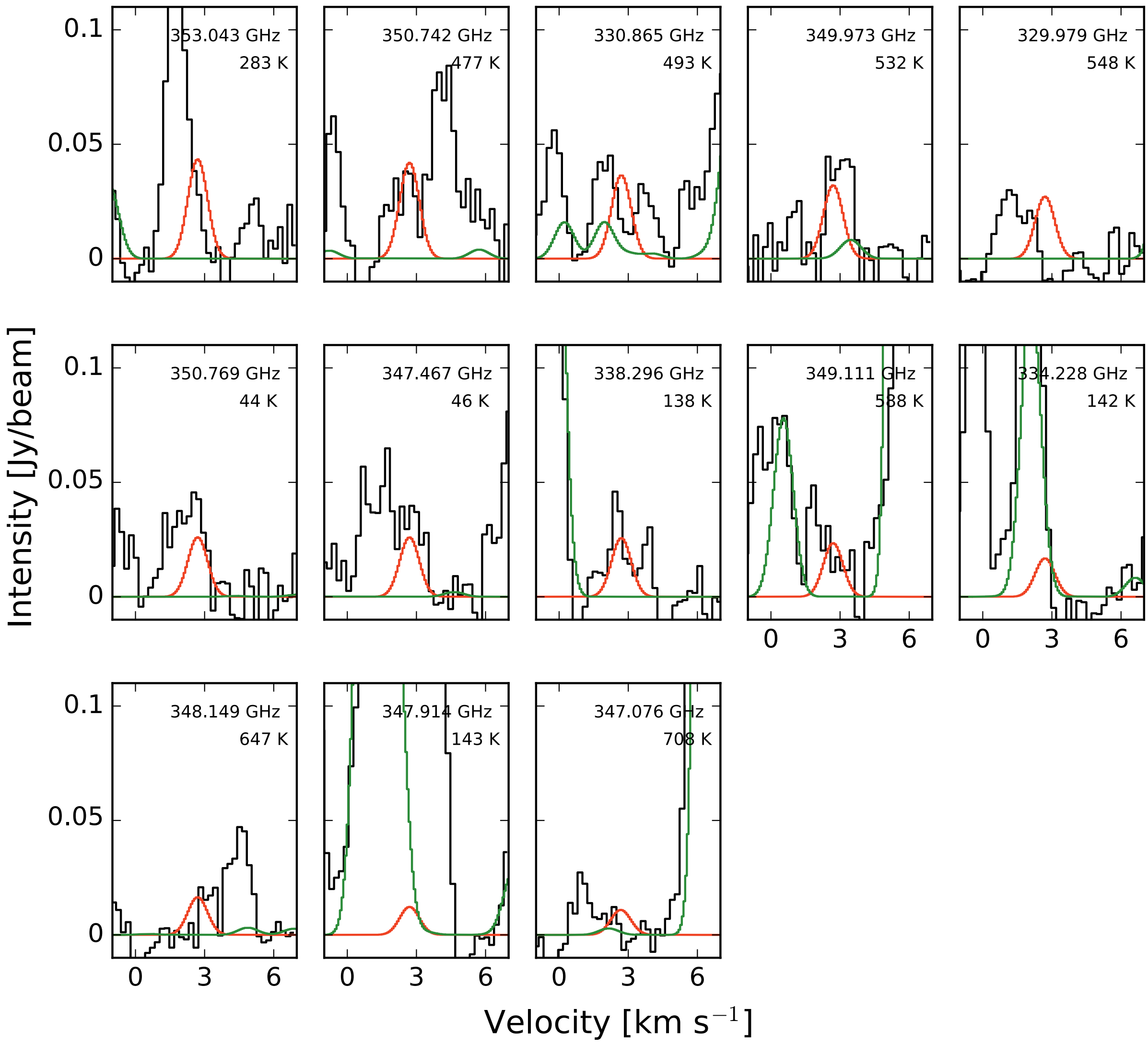

Fig. A.1. continued.

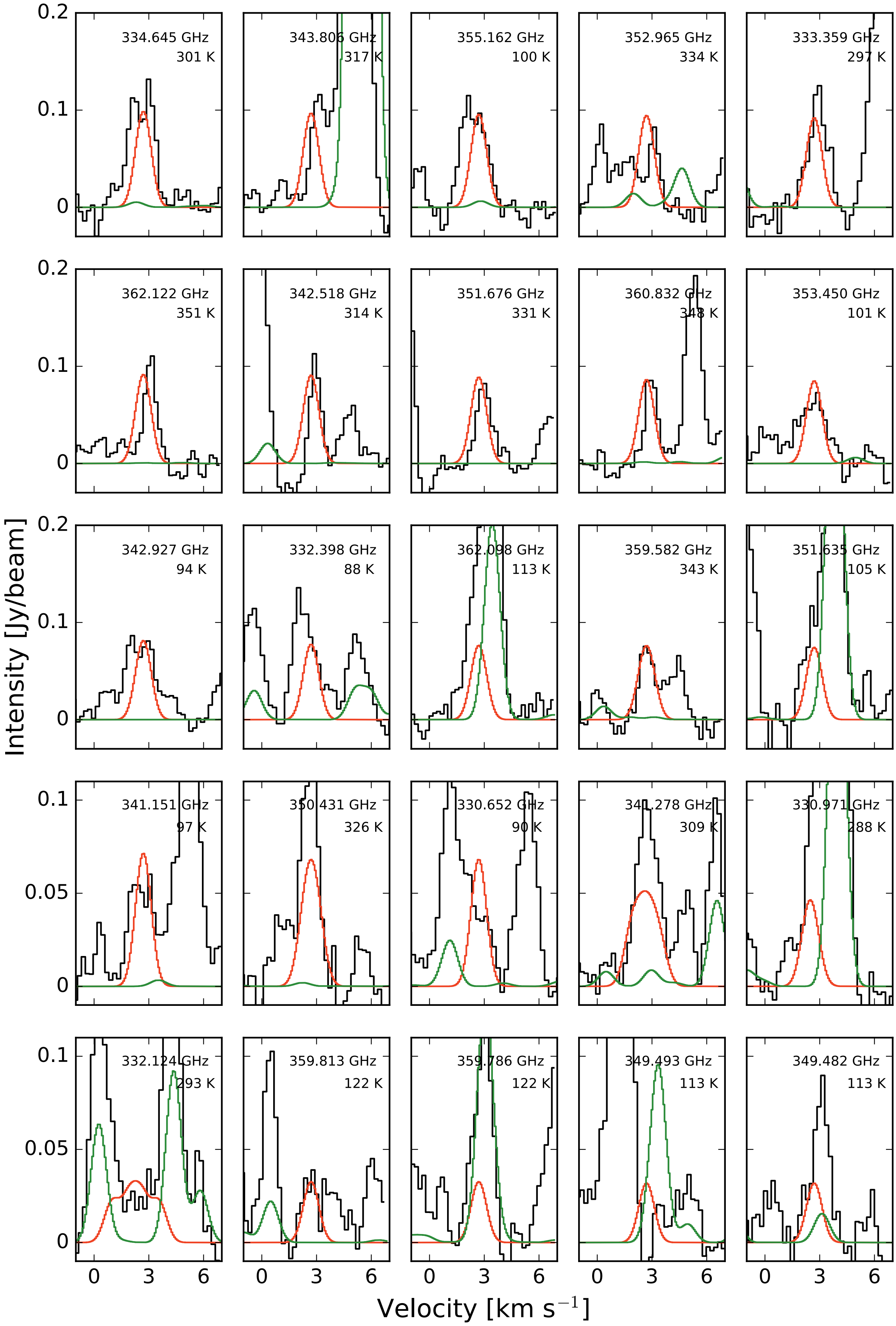

Fig. A.2. Propanal (C_2H_5CHO): synthetic spectrum in red and reference model in green superimposed onto observed spectrum.

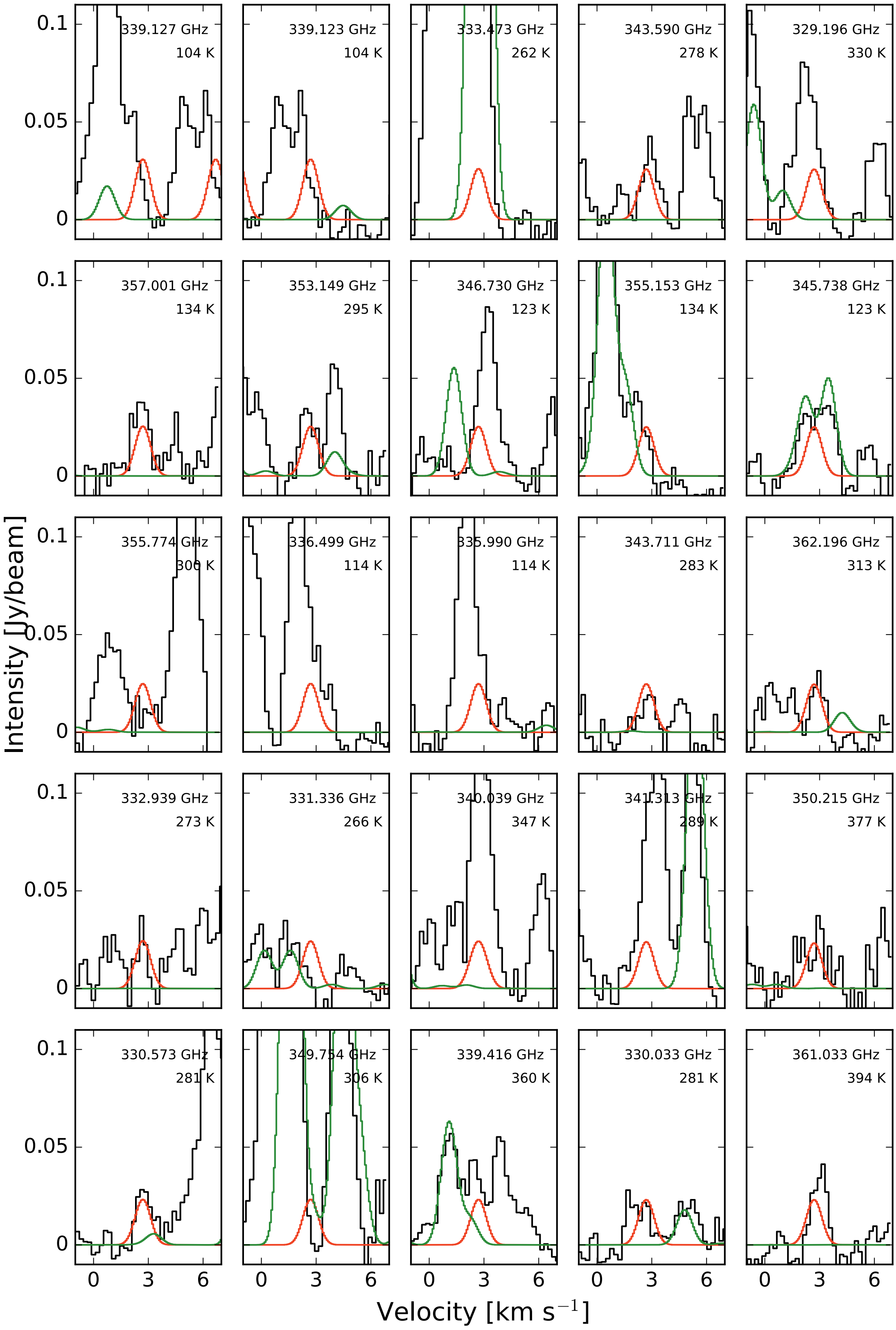

Fig. A.2. continued.

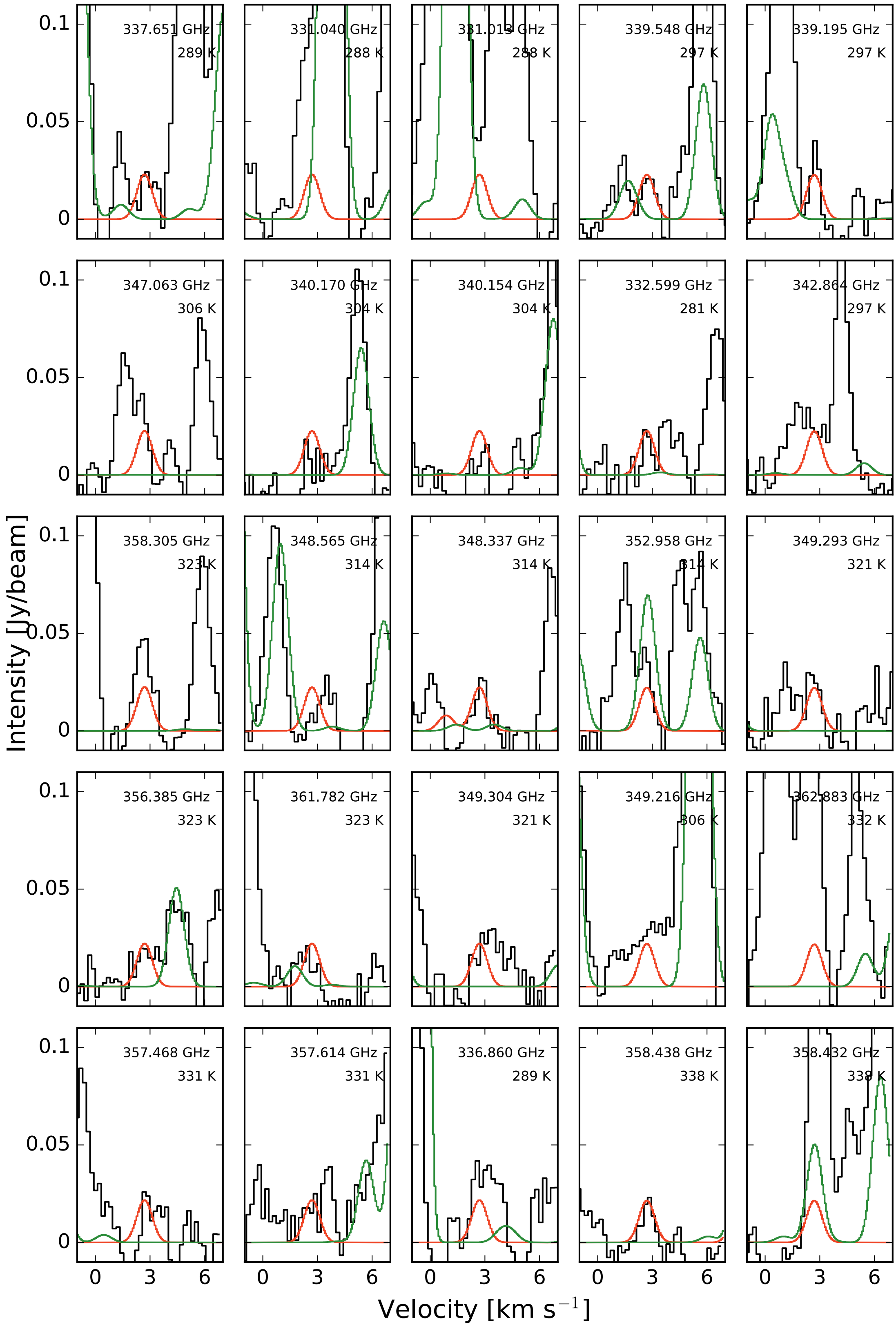

Fig. A.2. continued.

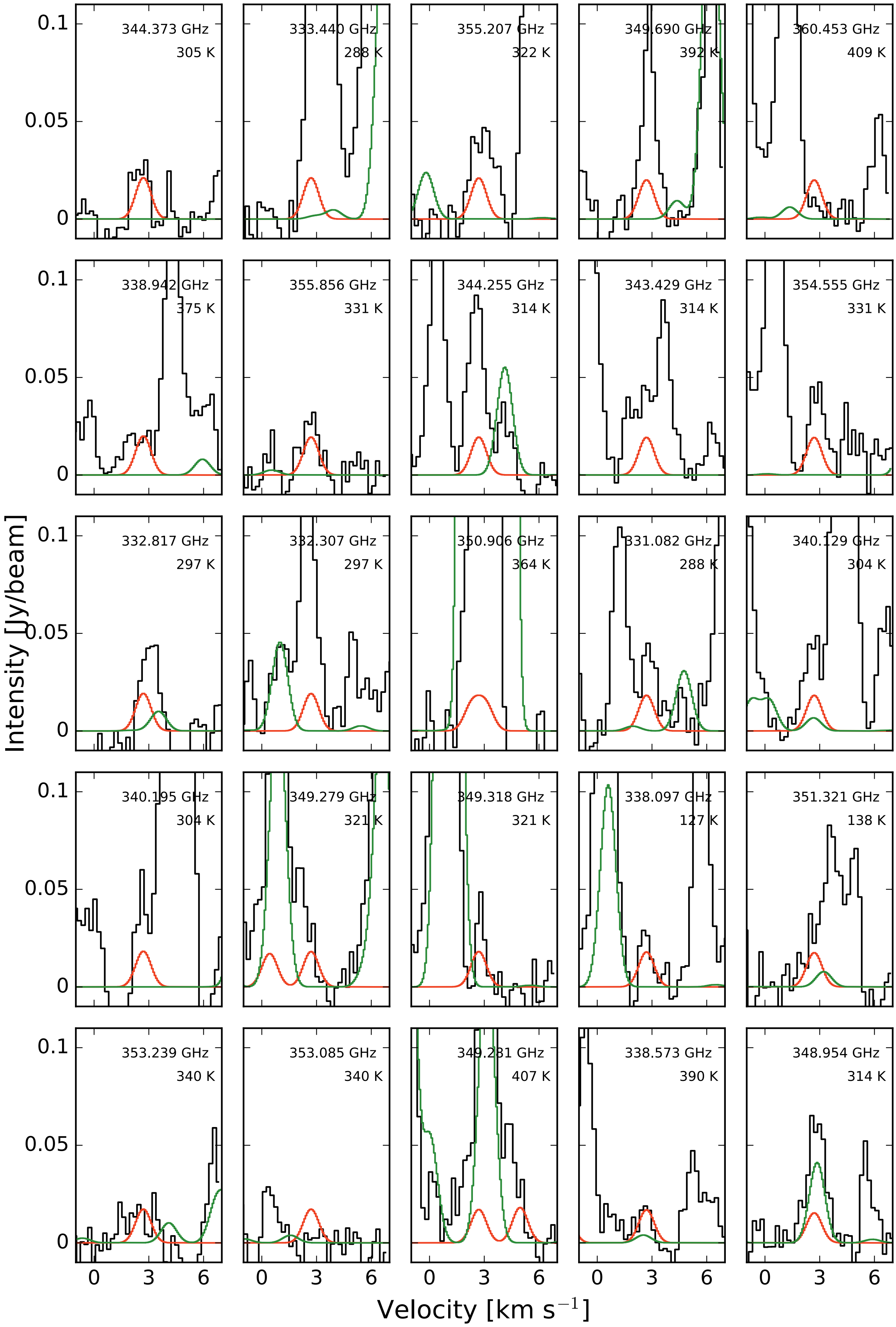

Fig. A.2. continued.

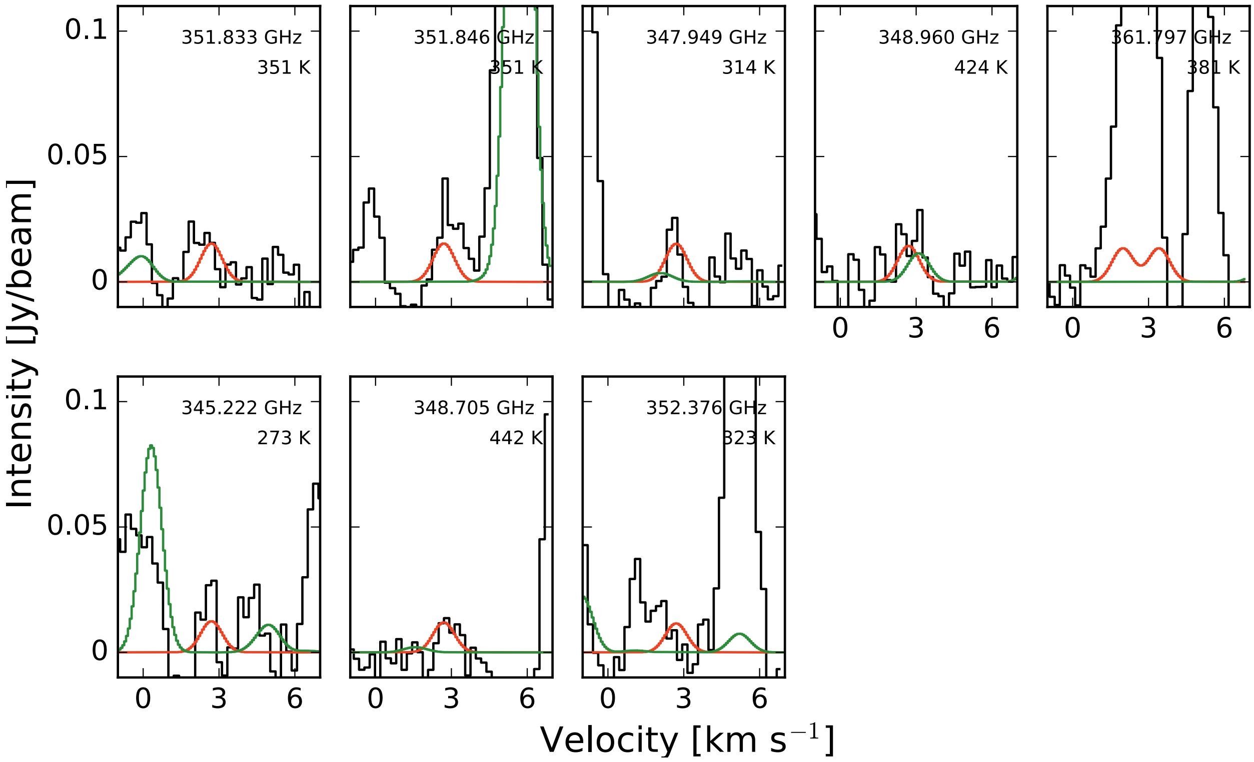

Fig. A.2. continued.

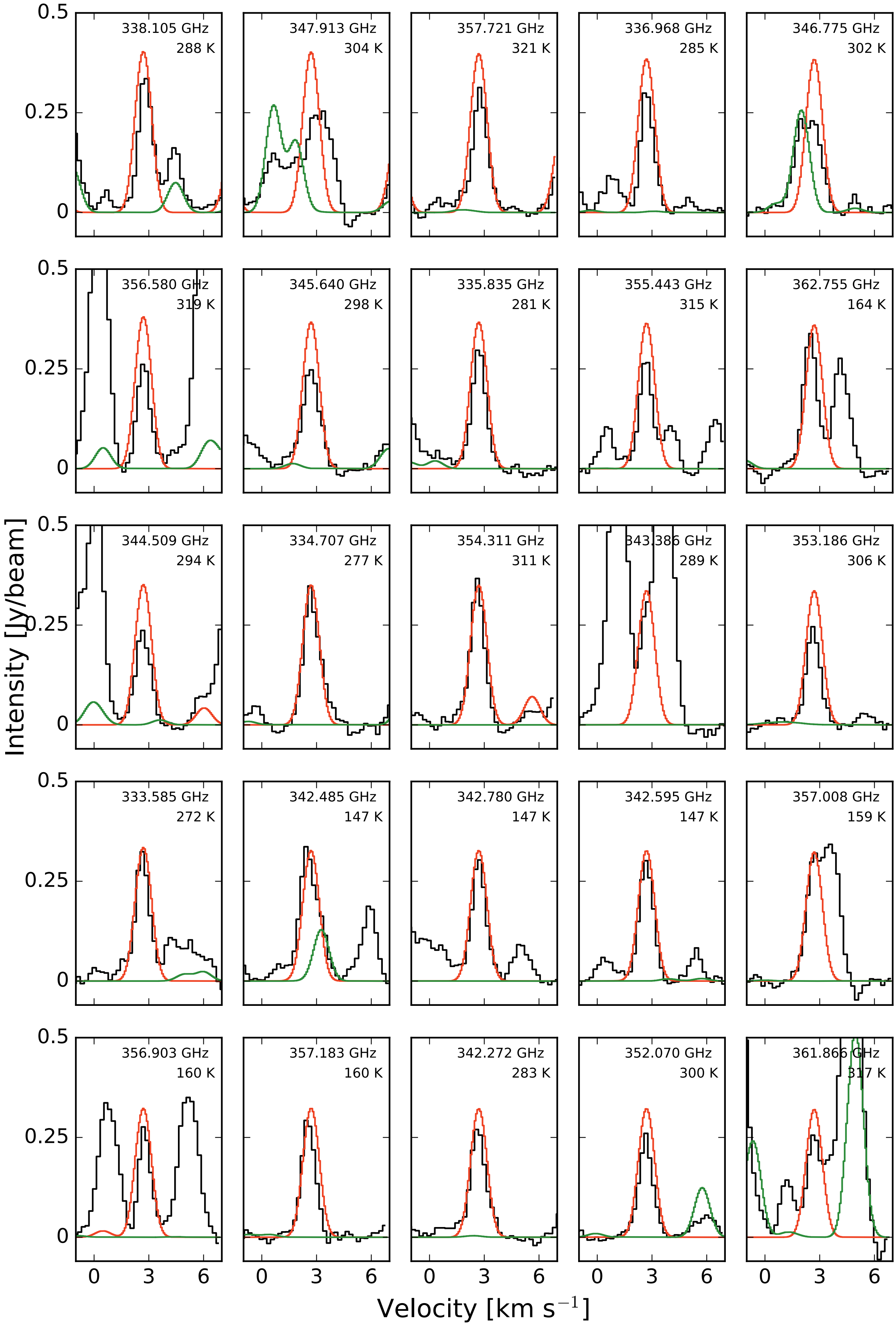

Fig. A.3. Acetone (CH_3COCH_3): synthetic spectrum in red and reference model in green superimposed onto observed spectrum.

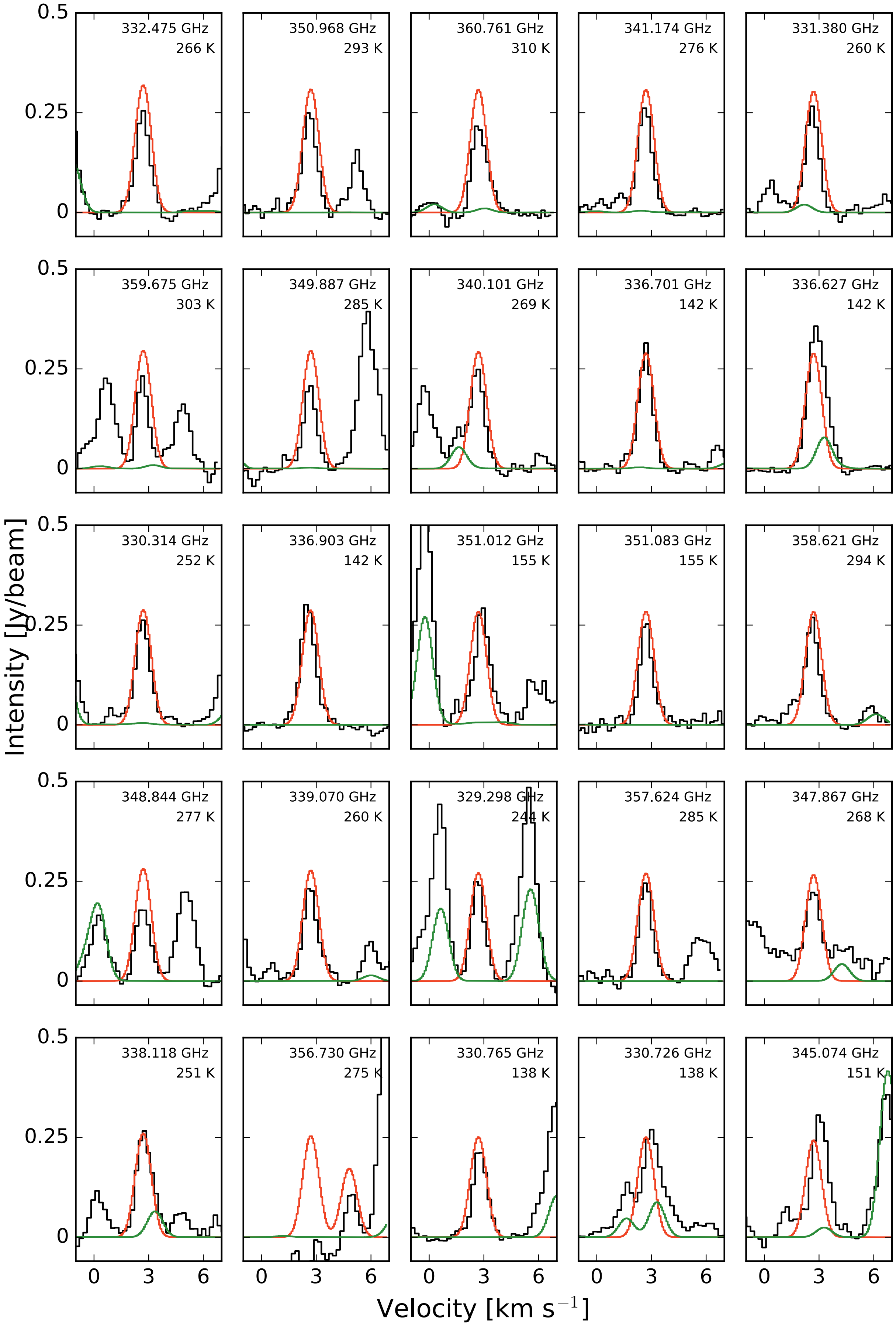

Fig. A.3. continued.

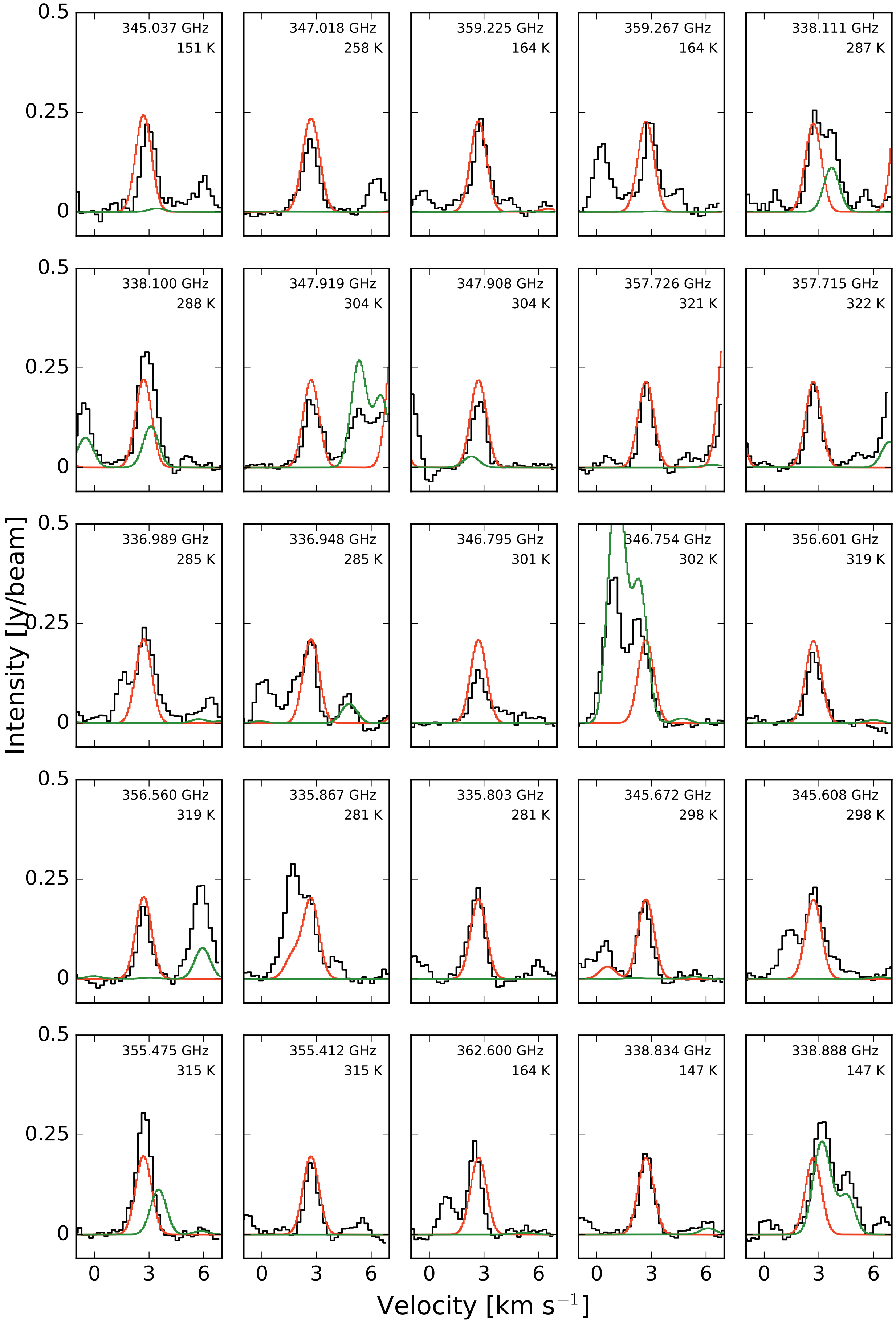

Fig. A.3. continued.

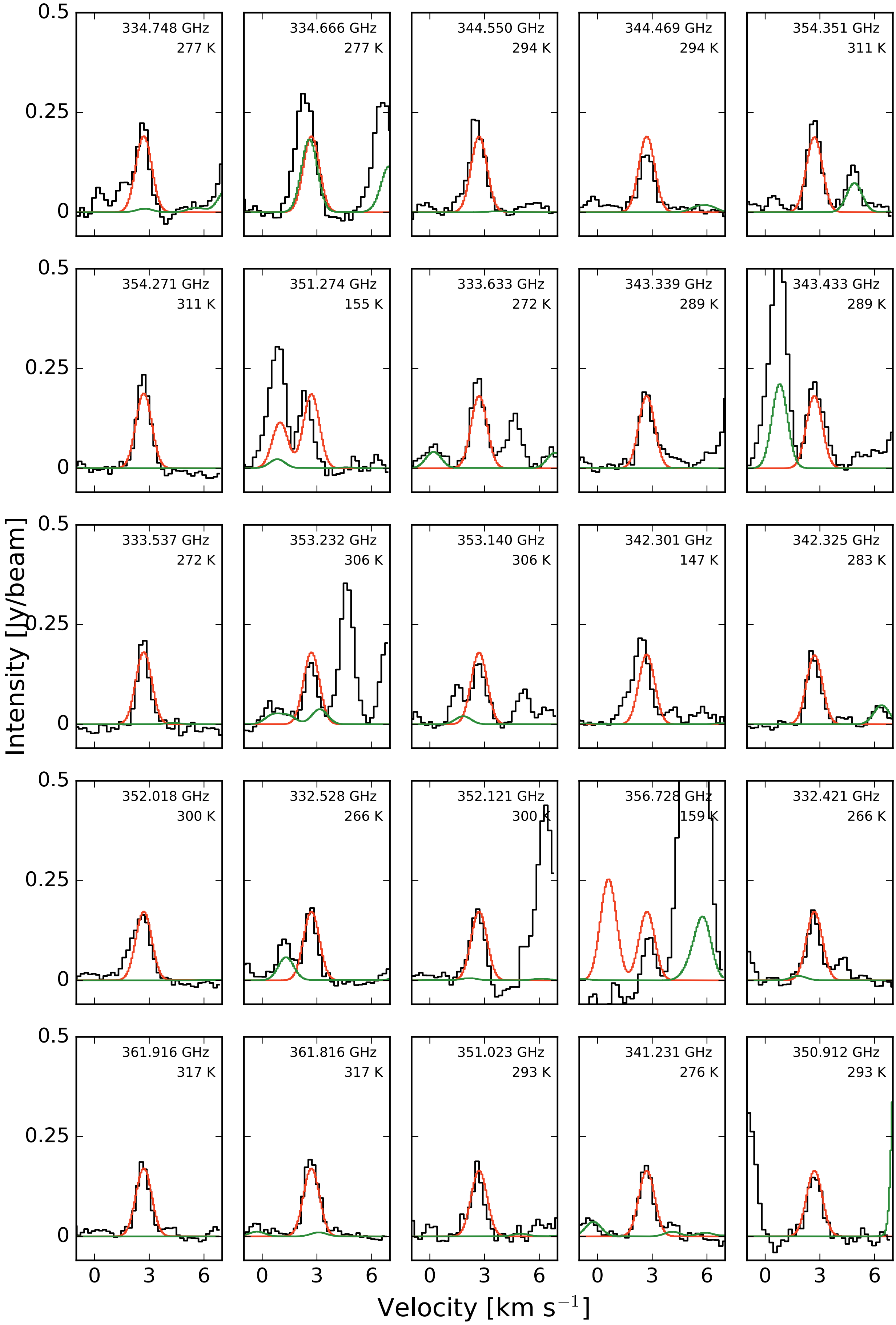

Fig. A.3. continued.

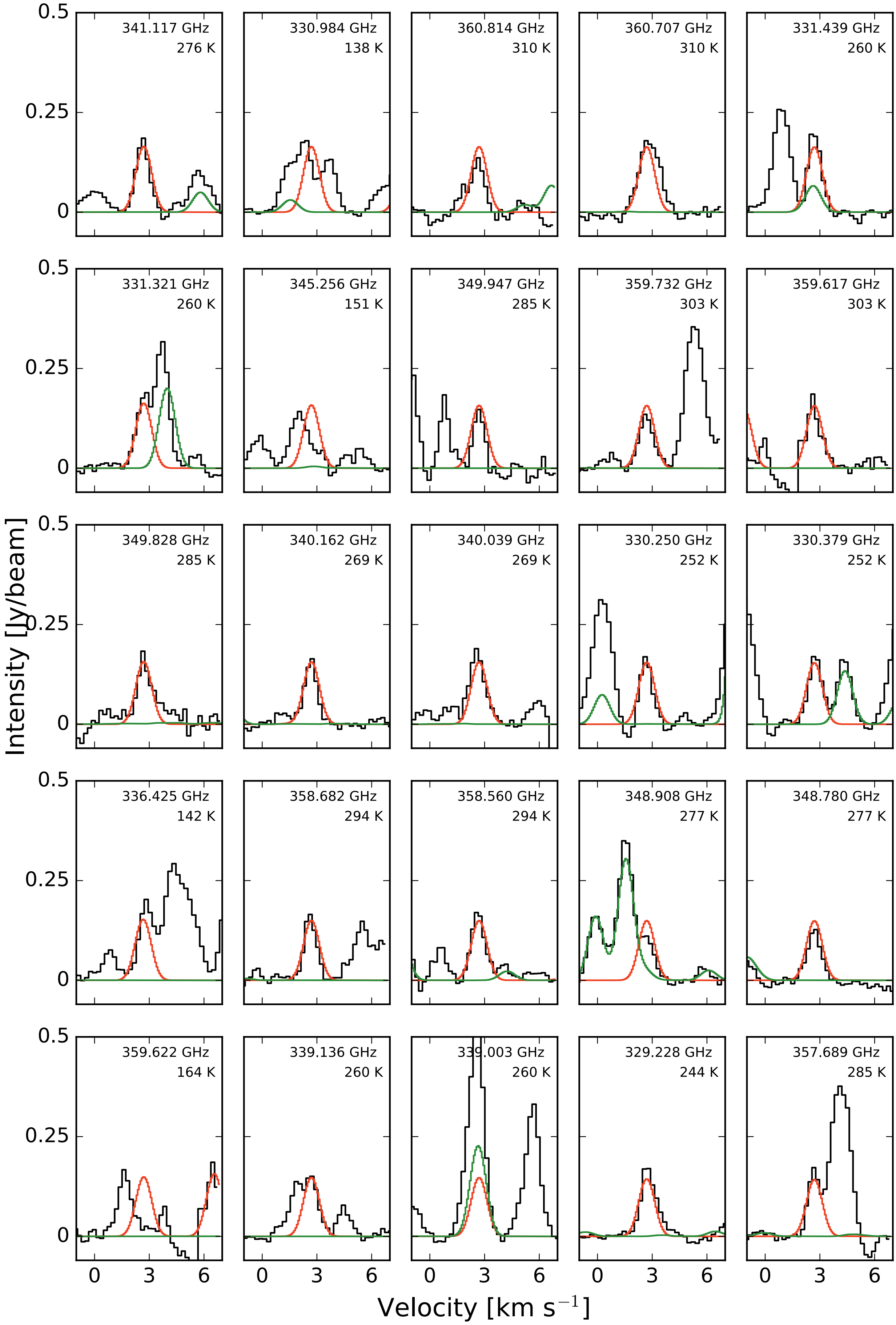

Fig. A.3. continued.

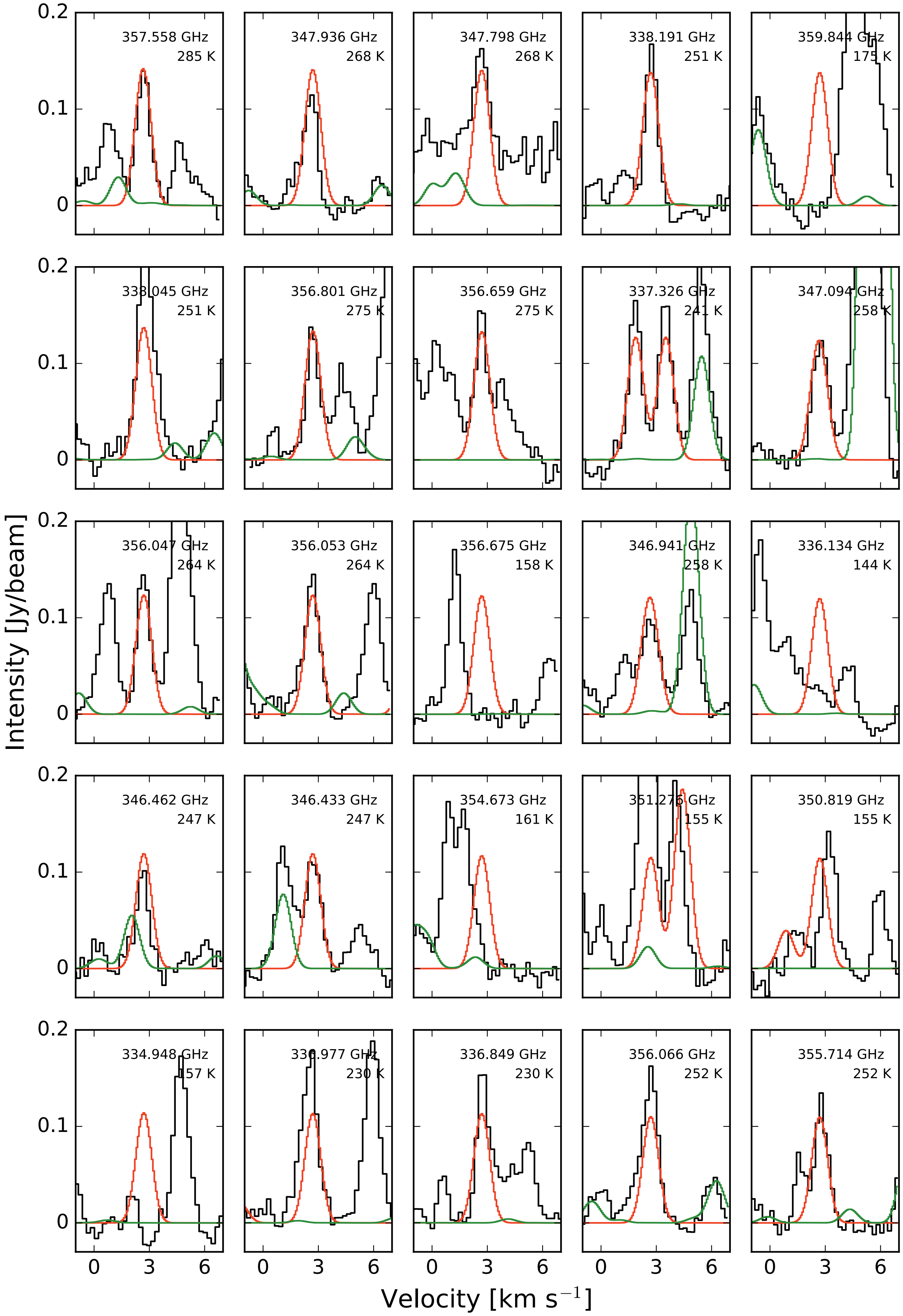

Fig. A.3. continued.

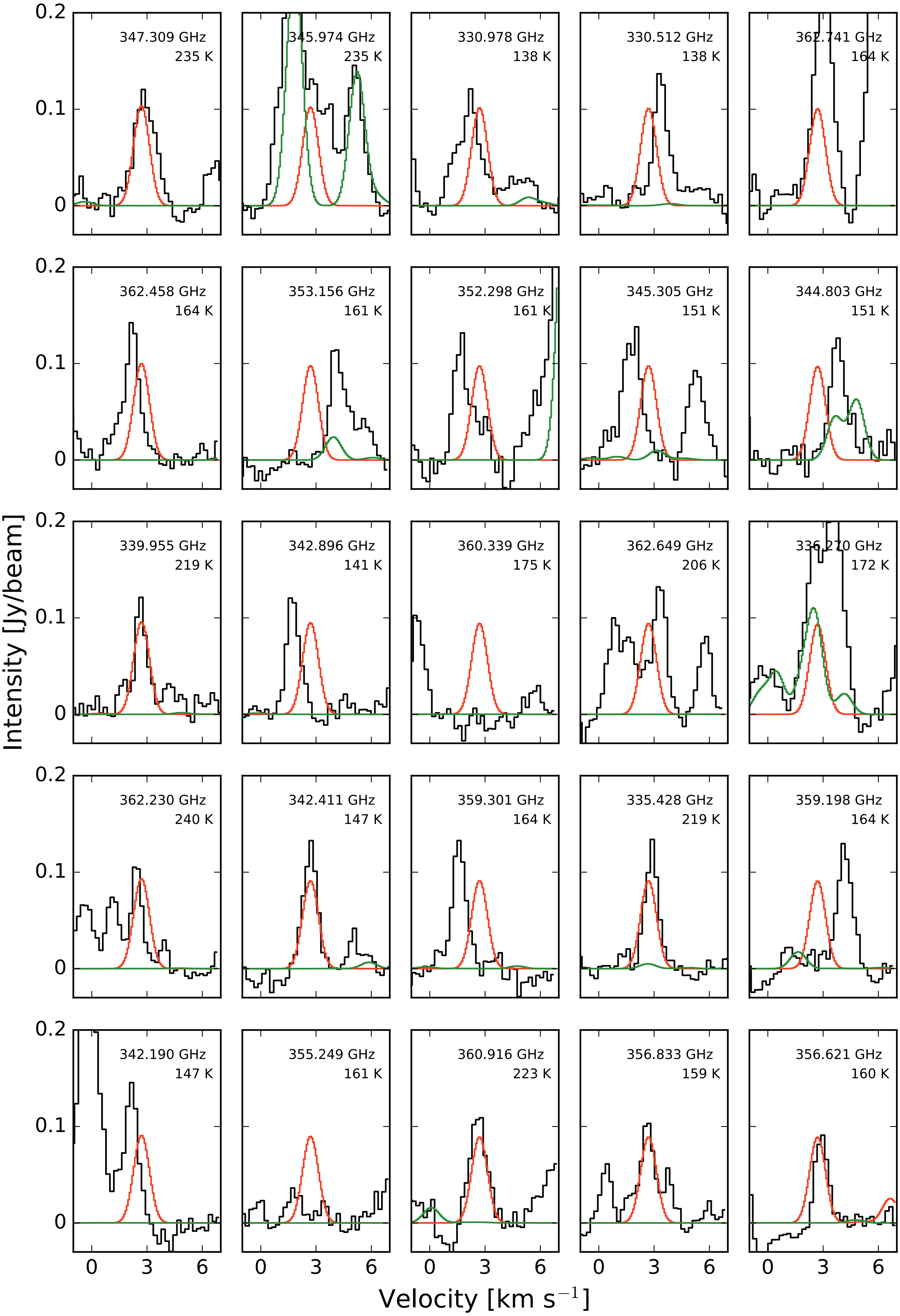

Fig. A.3. continued.

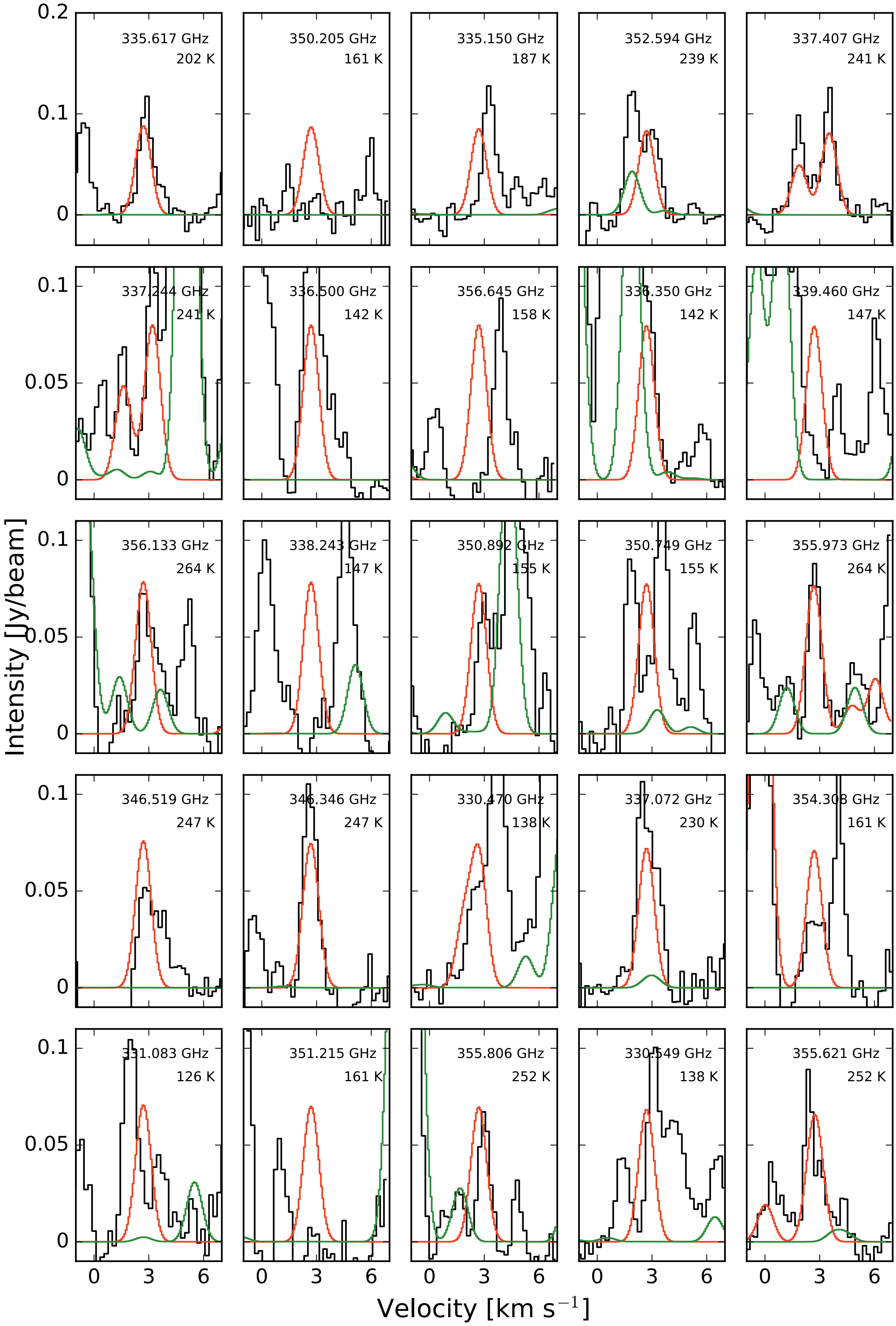

Fig. A.3. continued.

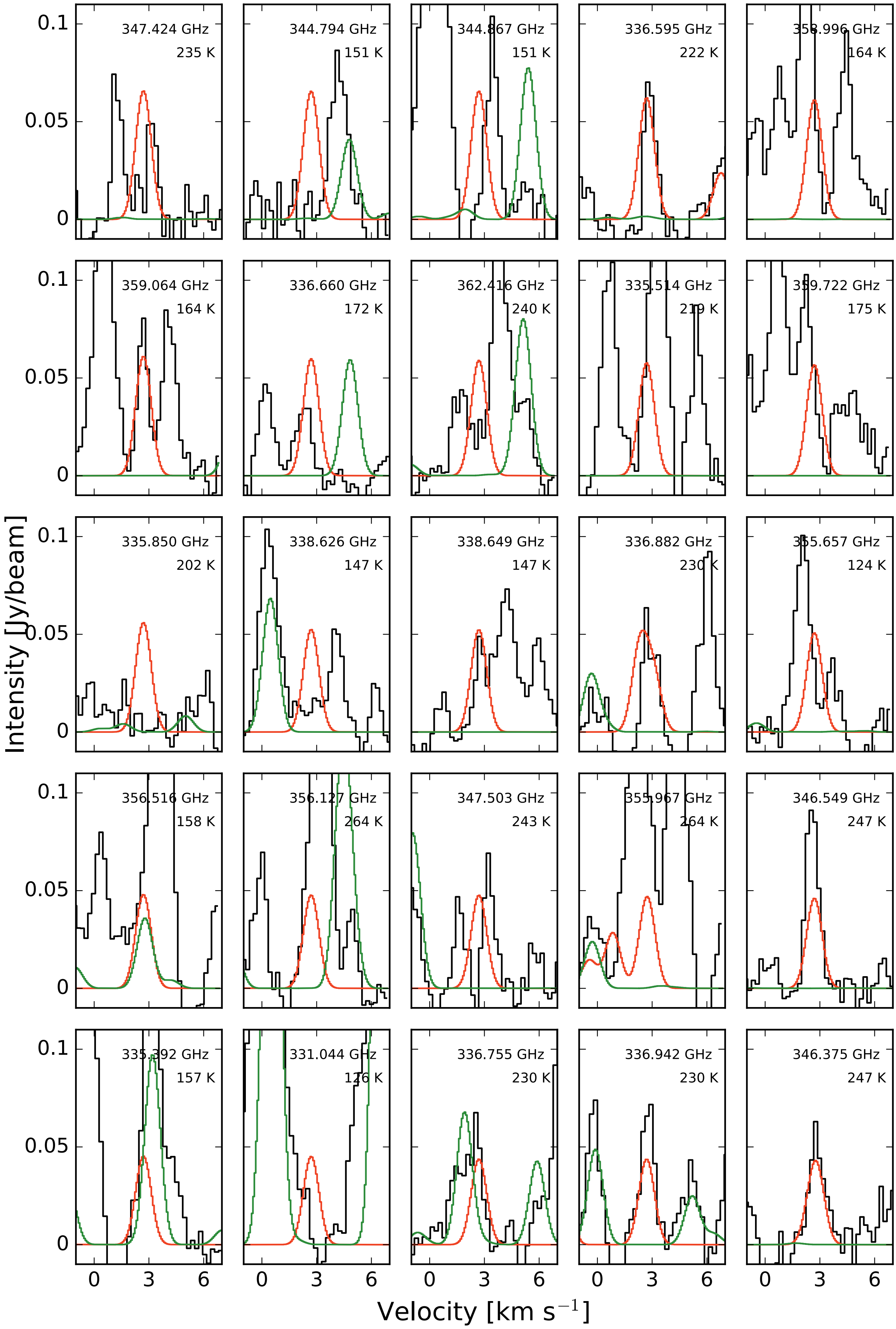

Fig. A.3. continued.

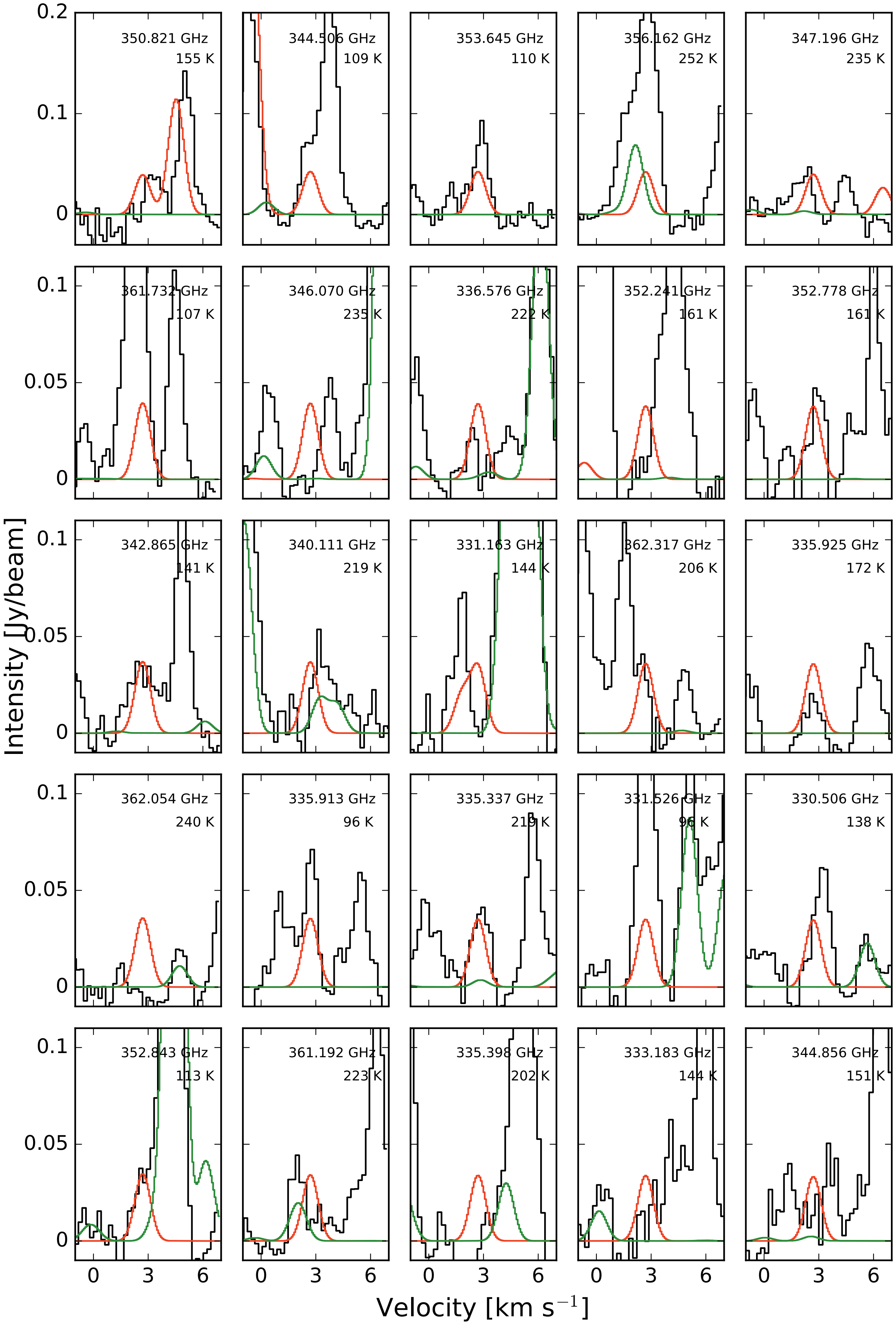

Fig. A.3. continued.

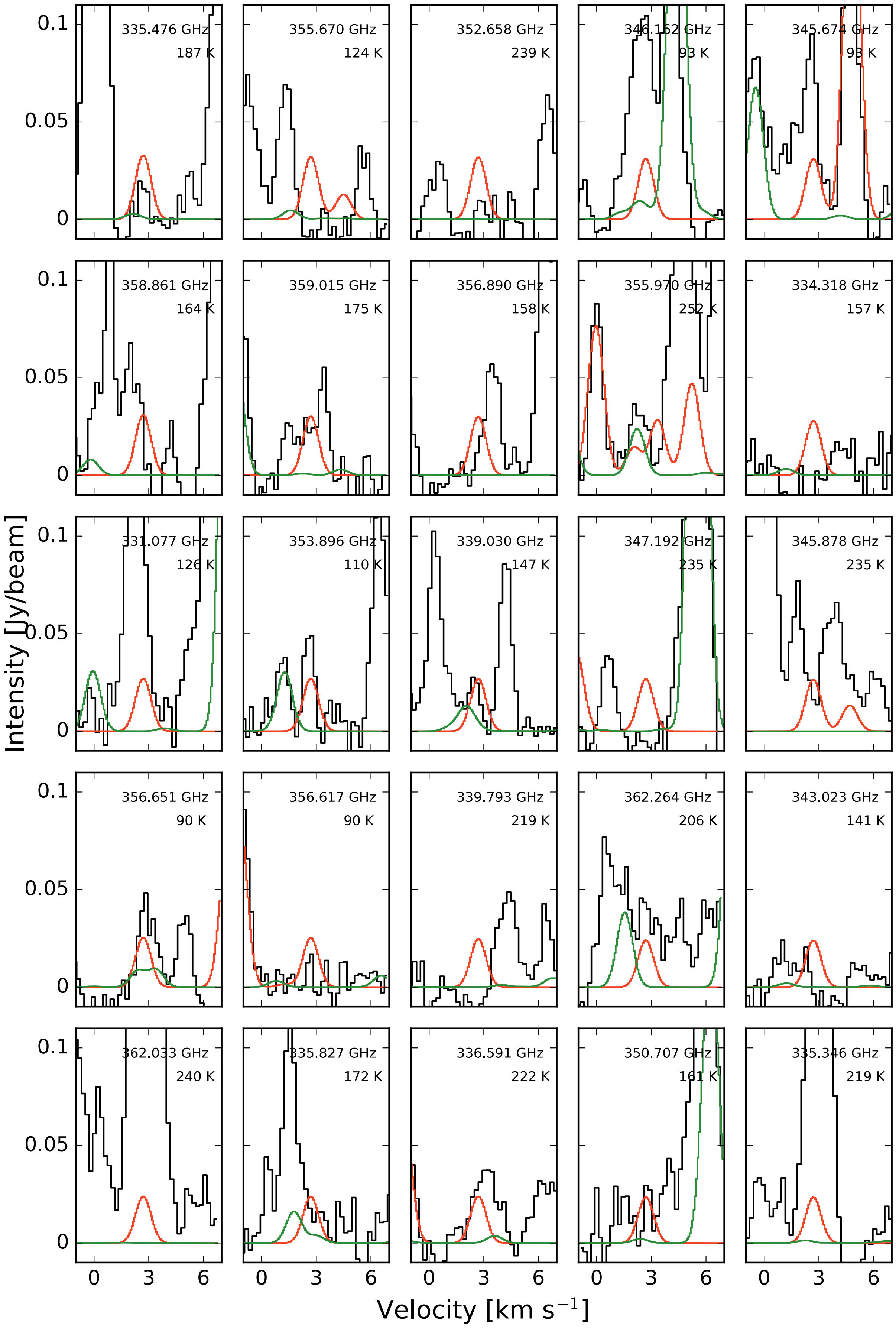

Fig. A.3. continued.

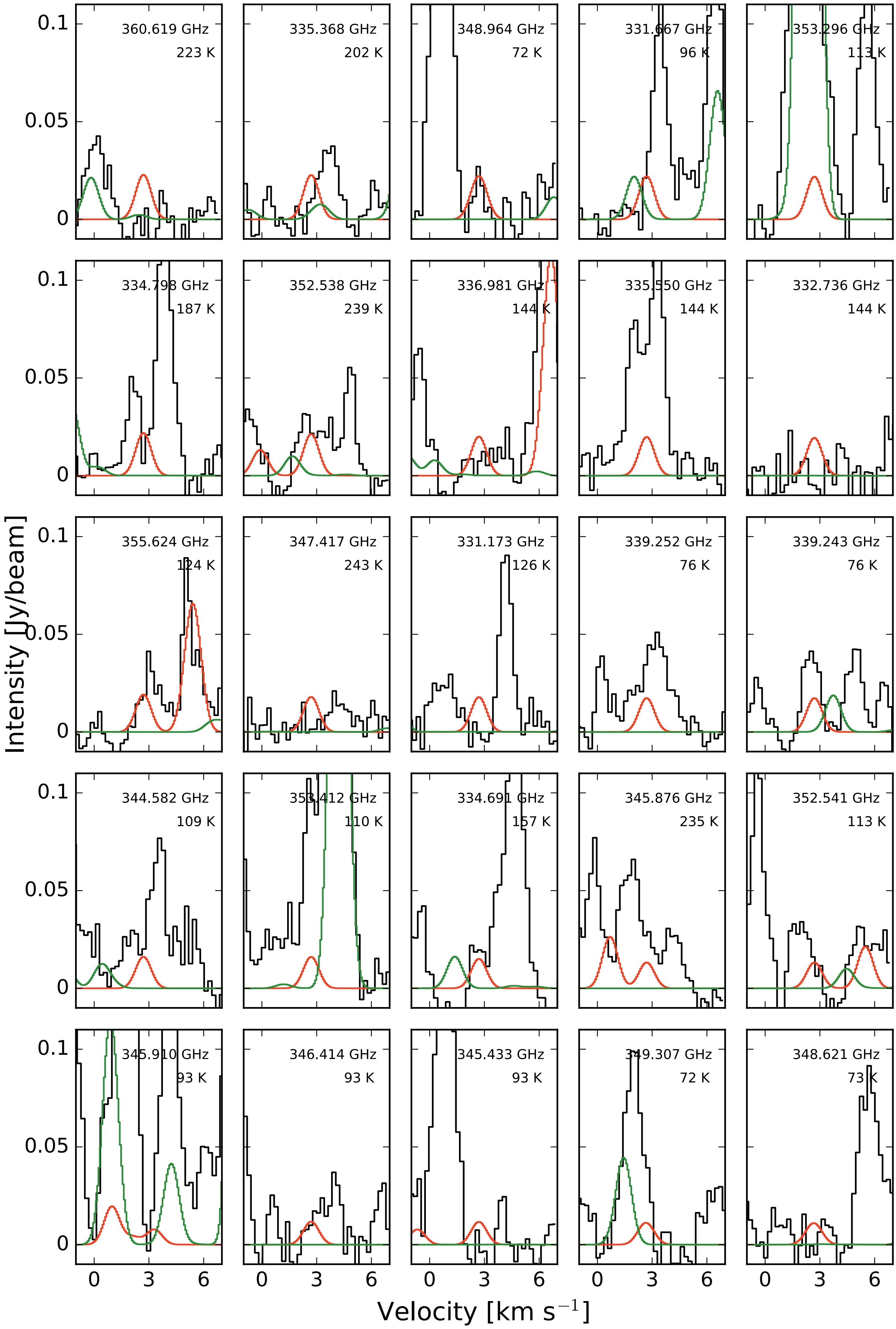

Fig. A.3. continued.

Appendix B: Detected lines

Table B.1. Catalog values for the detected propanal, ethylene oxide and acetone transitions and the integrated line strength of the synthetic spectrum.

Transition	Frequency [MHz]	$E_{\rm up}$ [K]	$\log_{10}(A_{\rm ul})$ [s^{-1}]	τ	$\int_{FWHM} I\,\delta v$ [J beam^{-1} km s^{-1}]	Detection level
			Ethylene oxide (c-C_2H_4O)			
$10_{2,8}-9_{3,7}$	329 744.34	95	−3.3018	5.33e-01	0.248	69
$10_{3,8}-9_{2,7}$	329 748.33	95	−3.3019	3.20e-01	0.147	41
$22_{5,17}-22_{4,18}$	331 651.32	441	−3.7416	2.58e-02	0.064	18
$22_{6,17}-22_{5,18}$	331 651.32	441	−3.7416	1.55e-02	0.064	18
$21_{4,17}-21_{3,18}$	332 345.92	392	−3.8096	1.87e-02	0.034	10
$21_{5,17}-21_{4,18}$	332 345.92	392	−3.8097	3.12e-02	0.034	10
$9_{4,5}-8_{5,4}$	336 561.39	90	−3.5297	1.71e-01	0.156	44
$11_{7,5}-10_{8,2}$	338 295.96	138	−4.5667	2.15e-02	0.027	8
$11_{1,10}-10_{2,9}$	338 771.98	104	−3.1922	4.00e-01	0.428	120
$11_{2,10}-10_{1,9}$	338 771.98	104	−3.1921	6.66e-01	0.428	120
$7_{6,1}-6_{5,2}$	341 730.22	63	−3.3675	2.38e-01	0.229	64
$9_{5,5}-8_{4,4}$	345 688.32	90	−3.4727	3.09e-01	0.249	70
$12_{0,12}-11_{1,11}$	347 843.06	111	−3.1026	7.99e-01	0.542	151
$12_{1,12}-11_{0,11}$	347 843.10	111	−3.1027	4.79e-01	0.542	151
$10_{3,7}-9_{4,6}$	348 966.62	102	−3.3039	4.50e-01	0.273	76
$10_{4,7}-9_{3,6}$	349 099.82	102	−3.3033	2.70e-01	0.246	69
$24_{6,18}-24_{5,19}$	349 972.85	532	−3.6332	1.57e-02	0.034	10
$24_{7,18}-24_{6,19}$	349 972.85	532	−3.6333	9.45e-03	0.034	10
$7_{7,1}-6_{6,0}$	350 303.48	66	−3.1488	6.08e-01	0.404	113
$7_{7,0}-6_{6,1}$	350 644.59	66	−3.1479	3.65e-01	0.291	81
$23_{5,18}-23_{4,19}$	350 741.95	477	−3.6859	1.23e-02	0.026	7
$23_{6,18}-23_{5,19}$	350 741.95	477	−3.6859	2.06e-02	0.026	7
$21_{3,18}-21_{2,19}$	352 033.68	376	−3.8513	1.73e-02	0.031	9
$21_{4,18}-21_{3,19}$	352 033.68	376	−3.8513	2.88e-02	0.031	9
$20_{2,18}-20_{1,19}$	352 570.56	328	−3.9971	2.87e-02	0.046	13
$20_{3,18}-20_{2,19}$	352 570.56	328	−3.9971	1.72e-02	0.046	13
$11_{2,9}-10_{3,8}$	357 909.16	113	−3.1776	3.47e-01	0.371	104
$11_{3,9}-10_{2,8}$	357 909.70	113	−3.1776	5.78e-01	0.531	149
$8_{6,3}-7_{5,2}$	361 519.42	78	−3.4205	1.90e-01	0.194	54
			Propanal (C_2H_5CHO)			
$32_{5,28}-31_{5,27}$	330 033.48	281	−3.2366	2.04e-02	0.013	4
$32_{4,28}-31_{4,27}$	330 572.90	281	−3.2344	2.04e-02	0.022	6
$13_{9,5}-12_{8,4}$	330 651.76	90	−3.3400	3.05e-02	0.042	12
$13_{9,4}-12_{8,5}$	330 651.76	90	−3.3400	3.05e-02	0.042	12
$31_{7,25}-30_{7,24}$	332 598.70	281	−3.2339	1.96e-02	0.012	3
$31_{5,26}-30_{5,25}$	332 939.34	273	−3.2271	2.12e-02	0.019	5
$35_{1,34}-34_{2,33}$	333 358.91	297	−3.2007	2.08e-02	0.089	25
$35_{2,34}-34_{2,33}$	333 358.92	297	−3.2123	2.03e-02	0.089	25
$35_{1,34}-34_{1,33}$	333 358.93	297	−3.2123	2.03e-02	0.089	25
$35_{2,34}-34_{1,33}$	333 358.95	297	−3.2007	2.08e-02	0.089	25
$32_{6,27}-31_{6,26}$	337 650.97	289	−3.2096	1.94e-02	0.015	4
$20_{6,14}-19_{5,15}$	338 096.89	127	−3.6845	1.50e-02	0.020	5
$32_{15,17}-31_{15,16}$	338 572.87	390	−3.2943	7.07e-03	0.013	4
$32_{15,18}-31_{15,17}$	338 572.87	390	−3.2943	7.07e-03	0.013	4
$33_{5,29}-32_{5,28}$	339 194.57	297	−3.2004	1.90e-02	0.020	6
$33_{4,29} - 32_{4,28}$	339 547.63	297	−3.1990	1.90e-02	0.017	5
$33_{5,29}-32_{4,28}$	340 164.32	297	−3.3742	1.27e-02	0.020	6
$14_{9,6}-13_{8,5}$	341 151.22	97	−3.3271	3.00e-02	0.052	15
$14_{9,5}-13_{8,6}$	341 151.23	97	−3.3271	3.00e-02	0.052	15
$35_{2,33}-34_{3,32}$	341 277.32	309	−3.2188	1.73e-02	0.084	23
$35_{3,33}-34_{3,32}$	341 277.92	309	−3.1853	1.87e-02	0.084	23
$35_{2,33}-34_{2,32}$	341 278.36	309	−3.1853	1.87e-02	0.084	23
$35_{3,33}-34_{2,32}$	341 278.96	309	−3.2188	1.73e-02	0.084	23
$20_{5,15}-19_{4,16}$	341 279.21	122	−3.9480	8.36e-03	0.029	8
$36_{1,35}-35_{2,34}$	342 518.47	314	−3.1633	1.94e-02	0.057	16

Notes. Due to line contamination, the integrated line strength is given for the FWHM of the Gaussian function.

Table B.1. continued.

Transition	Frequency [MHz]	E_{up} [K]	$\log_{10}(A_{\mathrm{ul}})$ [s^{-1}]	τ	$\int_{FWHM} I\,\delta v$ [J beam^{-1} km s^{-1}]	Detection level
$36_{2,35}-35_{2,34}$	342 518.47	314	–3.1767	1.88e-02	0.057	16
$36_{1,35}-35_{1,34}$	342 518.48	314	–3.1767	1.88e-02	0.057	16
$36_{2,35}-35_{1,34}$	342 518.49	314	–3.1633	1.94e-02	0.057	16
$12_{10,2}-11_{9,3}$	342 926.51	94	–3.2160	3.40e-02	0.072	20
$12_{10,3}-11_{9,2}$	342 926.51	94	–3.2160	3.40e-02	0.072	20
$31_{6,25}-30_{6,24}$	343 589.54	278	–3.1841	2.11e-02	0.027	8
$31_{7,24}-30_{7,23}$	343 711.33	283	–3.1880	2.01e-02	0.014	4
$37_{0,37}-36_{1,36}$	343 805.93	317	–3.1164	2.15e-02	0.072	20
$37_{1,37}-36_{1,36}$	343 805.93	317	–3.1679	1.91e-02	0.072	20
$37_{0,37}-36_{0,36}$	343 805.93	317	–3.1679	1.91e-02	0.072	20
$37_{1,37}-36_{0,36}$	343 805.93	317	–3.1164	2.15e-02	0.072	20
$32_{8,25}-31_{8,24}$	344 372.65	305	–3.1927	1.71e-02	0.024	7
$34_{4,30}-33_{5,29}$	347 948.63	314	–3.3326	1.20e-02	0.011	3
$34_{5,30}-33_{5,29}$	348 337.20	314	–3.1652	1.76e-02	0.017	5
$35_{4,32}-34_{4,31}$	349 293.49	321	–3.1583	1.74e-02	0.023	6
$35_{4,32}-34_{3,31}$	349 318.44	321	–3.2457	1.42e-02	0.021	6
$36_{2,34}-35_{3,33}$	350 430.33	326	–3.1805	1.61e-02	0.111	31
$36_{3,34}-35_{3,33}$	350 430.67	326	–3.1504	1.73e-02	0.111	31
$36_{2,34}-35_{2,33}$	350 430.92	326	–3.1504	1.73e-02	0.111	31
$36_{3,34}-35_{2,33}$	350 431.26	326	–3.1805	1.61e-02	0.111	31
$37_{1,36}-36_{2,35}$	351 676.10	331	–3.1270	1.80e-02	0.050	14
$37_{2,36}-36_{2,35}$	351 676.11	331	–3.1420	1.74e-02	0.050	14
$37_{1,36}-36_{1,35}$	351 676.11	331	–3.1420	1.74e-02	0.050	14
$37_{2,36}-36_{1,35}$	351 676.11	331	–3.1270	1.80e-02	0.050	14
$38_{0,38}-37_{1,37}$	352 965.05	334	–3.0815	1.98e-02	0.047	13
$38_{1,38}-37_{1,37}$	352 965.05	334	–3.1334	1.76e-02	0.047	13
$38_{0,38}-37_{0,37}$	352 965.05	334	–3.1334	1.76e-02	0.047	13
$38_{1,38}-37_{0,37}$	352 965.05	334	–3.0815	1.98e-02	0.047	13
$32_{6,26}-31_{6,25}$	353 148.80	295	–3.1484	1.95e-02	0.029	8
$13_{10,3}-12_{9,4}$	353 450.35	101	–3.2084	3.34e-02	0.060	17
$33_{9,25}-32_{9,24}$	354 555.43	331	–3.1598	1.47e-02	0.037	10
$11_{11,0}-10_{10,1}$	355 162.35	100	–3.0902	3.74e-02	0.083	23
$11_{11,1}-10_{10,0}$	355 162.35	100	–3.0902	3.74e-02	0.083	23
$33_{9,24}-32_{9,23}$	355 856.08	331	–3.1550	1.47e-02	0.023	7
$34_{6,29}-33_{6,28}$	356 384.80	323	–3.1379	1.67e-02	0.016	5
$20_{7,13}-19_{6,14}$	357 000.67	134	–3.5090	1.92e-02	0.032	9
$35_{5,31}-34_{5,30}$	357 467.93	331	–3.1310	1.63e-02	0.012	3
$35_{4,31}-34_{4,30}$	357 613.69	331	–3.1304	1.63e-02	0.016	5
$34_{5,29}-33_{5,28}$	358 305.47	323	–3.1306	1.68e-02	0.037	10
$36_{3,33}-35_{3,32}$	358 438.34	338	–3.1242	1.60e-02	0.015	4
$37_{2,35}-36_{3,34}$	359 581.63	343	–3.1434	1.50e-02	0.060	17
$37_{3,35}-36_{3,34}$	359 581.82	343	–3.1164	1.59e-02	0.060	17
$37_{2,35}-36_{2,34}$	359 581.97	343	–3.1164	1.59e-02	0.060	17
$37_{3,35}-36_{2,34}$	359 582.16	343	–3.1434	1.50e-02	0.060	17
$18_{8,10}-17_{7,11}$	359 812.79	122	–3.3969	2.43e-02	0.030	8
$38_{1,37}-37_{2,36}$	360 831.75	348	–3.0917	1.66e-02	0.059	16
$38_{2,37}-37_{2,36}$	360 831.75	348	–3.1082	1.60e-02	0.059	16
$38_{1,37}-37_{1,36}$	360 831.75	348	–3.1082	1.60e-02	0.059	16
$38_{2,37}-37_{1,36}$	360 831.75	348	–3.0917	1.66e-02	0.059	16
$34_{13,22}-33_{13,21}$	361 033.21	394	–3.1711	8.54e-03	0.028	8
$34_{13,21}-33_{13,20}$	361 033.31	394	–3.1711	8.54e-03	0.028	8
$39_{0,39}-38_{1,38}$	362 122.12	351	–3.0475	1.82e-02	0.067	19
$39_{0,39}-38_{0,38}$	362 122.12	351	–3.0999	1.61e-02	0.067	19
$39_{1,39}-38_{0,38}$	362 122.12	351	–3.0475	1.82e-02	0.067	19
$39_{1,39}-38_{1,38}$	362 122.12	351	–3.0999	1.61e-02	0.067	19
$33_{6,27}-32_{6,26}$	362 196.30	313	–3.1159	1.80e-02	0.019	5
Acetone (CH_3COCH_3)						
$26_{8,18}-25_{9,17}$ EA	329 228.06	244	–2.9657	3.38e-02	0.130	36
$26_{9,18}-25_{8,17}$ EA	329 228.06	244	–2.9657	3.38e-02	0.130	36

Table B.1. continued.

Transition	Frequency [MHz]	$E_{\rm up}$ [K]	$\log_{10}(A_{\rm ul})$ [s^{-1}]	τ	$\int_{FWHM} I\,\delta v$ [J beam^{-1} km s^{-1}]	Detection level
$26_{8,18}-25_{9,17}$ AE	329 228.14	244	−2.9657	1.69e-02	0.130	36
$26_{9,18}-25_{8,17}$ AE	329 228.14	244	−2.9657	5.07e-02	0.130	36
$26_{8,18}-25_{9,17}$ EE	329 298.16	244	−2.9656	1.35e-01	0.178	50
$26_{9,18}-25_{8,17}$ EE	329 298.16	244	−2.9656	1.35e-01	0.178	50
$14_{7,8}-13_{4,9}$ AA	329 367.94	80	−4.0975	1.27e-02	0.118	33
$26_{8,18}-25_{9,17}$ AA	329 368.09	244	−2.9654	5.07e-02	0.117	33
$26_{9,18}-25_{8,17}$ AA	329 368.10	244	−2.9654	8.45e-02	0.117	33
$27_{7,20}-26_{8,19}$ EA	330 250.07	252	−2.9233	3.60e-02	0.114	32
$27_{8,20}-26_{7,19}$ EA	330 250.07	252	−2.9233	3.60e-02	0.114	32
$27_{7,20}-26_{8,19}$ AE	330 250.13	252	−2.9233	5.40e-02	0.114	32
$27_{8,20}-26_{7,19}$ AE	330 250.13	252	−2.9232	1.80e-02	0.114	32
$51_{13,38}-51_{13,39}$ EE	330 250.15	875	−3.5999	2.36e-04	0.114	32
$51_{14,38}-51_{13,39}$ EE	330 250.15	875	−3.2461	5.32e-04	0.114	32
$51_{13,38}-51_{12,39}$ EE	330 250.15	875	−3.2461	5.32e-04	0.114	32
$51_{14,38}-51_{12,39}$ EE	330 250.15	875	−3.5999	2.36e-04	0.114	32
$27_{7,20}-26_{8,19}$ EE	330 314.39	252	−2.9231	1.44e-01	0.198	55
$27_{8,20}-26_{7,19}$ EE	330 314.39	252	−2.9231	1.44e-01	0.198	55
$27_{7,20}-26_{8,19}$ AA	330 378.56	252	−2.9230	9.00e-02	0.122	34
$27_{8,20}-26_{7,19}$ AA	330 378.56	252	−2.9230	5.40e-02	0.122	34
$17_{15,3}-16_{14,2}$ AE	330 506.31	138	−2.8918	3.06e-02	0.035	10
$17_{15,2}-16_{14,3}$ AE	330 512.29	138	−2.8918	9.19e-02	0.038	11
$17_{15,3}-16_{14,3}$ EA	330 549.33	138	−2.8919	6.13e-02	0.057	16
$17_{15,2}-16_{14,2}$ EE	330 725.88	138	−2.8905	2.45e-01	0.207	58
$17_{15,3}-16_{14,3}$ EE	330 765.02	138	−2.8906	2.45e-01	0.153	43
$13_{3,10}-12_{2,11}$ EE	331 129.66	60	−4.7227	5.19e-03	0.015	4
$13_{4,10}-12_{1,11}$ EE	331 129.71	60	−4.7227	5.19e-03	0.015	4
$28_{6,22}-27_{7,21}$ EA	331 321.41	260	−2.8862	3.80e-02	0.148	41
$28_{7,22}-27_{6,21}$ EA	331 321.41	260	−2.8862	3.80e-02	0.148	41
$28_{6,22}-27_{7,21}$ AE	331 321.46	260	−2.8863	1.90e-02	0.148	41
$28_{7,22}-27_{6,21}$ AE	331 321.46	260	−2.8863	5.70e-02	0.148	41
$28_{7,22}-27_{7,21}$ EE	331 380.50	260	−3.0073	1.15e-01	0.191	53
$28_{6,22}-27_{7,21}$ EE	331 380.50	260	−3.4997	3.70e-02	0.191	53
$28_{6,22}-27_{6,21}$ EE	331 380.50	260	−3.0094	1.15e-01	0.191	53
$28_{7,22}-27_{6,21}$ EE	331 380.50	260	−3.4932	3.76e-02	0.191	53
$29_{5,24}-28_{5,23}$ EA	332 420.74	266	−2.8535	4.00e-02	0.116	33
$29_{6,24}-28_{6,23}$ EA	332 420.74	266	−2.8535	4.00e-02	0.116	33
$29_{5,24}-28_{5,23}$ AE	332 420.79	266	−2.8535	2.00e-02	0.116	33
$29_{6,24}-28_{6,23}$ AE	332 420.79	266	−2.8535	6.00e-02	0.116	33
$29_{5,24}-28_{5,23}$ EE	332 474.57	266	−3.4029	4.52e-02	0.185	52
$29_{5,24}-28_{6,23}$ EE	332 474.57	266	−2.9972	1.15e-01	0.185	52
$29_{6,24}-28_{6,23}$ EE	332 474.57	266	−3.4029	4.52e-02	0.185	52
$29_{6,24}-28_{5,23}$ EE	332 474.57	266	−2.9972	1.15e-01	0.185	52
$29_{6,24}-28_{6,23}$ AA	332 528.32	266	−2.8532	1.00e-01	0.125	35
$29_{5,24}-28_{5,23}$ AA	332 528.32	266	−2.8532	6.00e-02	0.125	35
$30_{4,26}-29_{5,25}$ EA	333 537.35	272	−2.8239	4.20e-02	0.139	39
$30_{5,26}-29_{4,25}$ EA	333 537.35	272	−2.8239	4.20e-02	0.139	39
$30_{5,26}-29_{5,25}$ AE	333 537.39	272	−2.8240	2.10e-02	0.139	39
$30_{4,26}-29_{4,25}$ AE	333 537.39	272	−2.8240	6.30e-02	0.139	39
$30_{4,26}-29_{4,25}$ EE	333 585.34	272	−4.7355	2.06e-03	0.235	66
$30_{5,26}-29_{4,25}$ EE	333 585.34	272	−2.8291	1.66e-01	0.235	66
$30_{4,26}-29_{5,25}$ EE	333 585.34	272	−2.8291	1.66e-01	0.235	66
$30_{5,26}-29_{5,25}$ EE	333 585.34	272	−4.7355	2.06e-03	0.235	66
$30_{4,26}-29_{5,25}$ AA	333 633.28	272	−2.8236	6.30e-02	0.170	48
$30_{5,26}-29_{4,25}$ AA	333 633.28	272	−2.8237	1.05e-01	0.170	48
$19_{13,7}-18_{12,6}$ AE	334 691.41	157	−3.2379	1.29e-02	0.018	5
$31_{3,28}-30_{3,27}$ EE	334 706.67	277	−3.2332	6.39e-02	0.255	71
$31_{3,28}-30_{4,27}$ EE	334 706.67	277	−2.9889	1.12e-01	0.255	71
$31_{4,28}-30_{4,27}$ EE	334 706.67	277	−3.2332	6.39e-02	0.255	71
$31_{4,28}-30_{3,27}$ EE	334 706.67	277	−2.9889	1.12e-01	0.255	71
$31_{3,28}-30_{4,27}$ AA	334 747.64	277	−2.7968	1.10e-01	0.149	42

Table B.1. continued.

Transition	Frequency [MHz]	$E_{\rm up}$ [K]	$\log_{10}(A_{\rm ul})$ [s^{-1}]	τ	$\int_{FWHM} I\,\delta v$ [J beam^{-1} km s^{-1}]	Detection level
$31_{3,28}-30_{4,27}$ AA	334 747.64	277	−2.7968	1.10e-01	0.160	45
$31_{4,28}-30_{3,27}$ AA	334 747.64	277	−2.7969	6.60e-02	0.149	42
$31_{4,28}-30_{3,27}$ AA	334 747.64	277	−2.7969	6.60e-02	0.160	45
$21_{13,9}-20_{12,8}$ EE	335 150.46	187	−3.3155	7.48e-02	0.059	16
$23_{12,11}-22_{13,10}$ AE	335 336.65	219	−3.2138	3.00e-02	0.033	9
$23_{12,11}-22_{13,10}$ EE	335 427.63	219	−3.2142	8.00e-02	0.087	24
$22_{13,10}-21_{12,9}$ EE	335 617.32	202	−3.2655	7.73e-02	0.075	21
$32_{2,30}-31_{3,29}$ EA	335 802.89	281	−2.7724	4.61e-02	0.167	47
$32_{3,30}-31_{2,29}$ EA	335 802.89	281	−2.7724	4.61e-02	0.167	47
$32_{2,30}-31_{2,29}$ AE	335 802.91	281	−2.7724	6.92e-02	0.167	47
$32_{3,30}-31_{3,29}$ AE	335 802.91	281	−2.7724	2.31e-02	0.167	47
$32_{2,30}-31_{3,29}$ EE	335 835.06	281	−3.1155	8.05e-02	0.219	61
$32_{2,30}-31_{2,29}$ EE	335 835.06	281	−3.0035	1.04e-01	0.219	61
$32_{3,30}-31_{3,29}$ EE	335 835.06	281	−3.0035	1.04e-01	0.219	61
$32_{3,30}-31_{2,29}$ EE	335 835.06	281	−3.1155	8.05e-02	0.219	61
$32_{3,30}-31_{3,29}$ AA	335 867.22	281	−2.7722	6.93e-02	0.156	44
$32_{2,30}-31_{2,29}$ AA	335 867.22	281	−2.7722	1.15e-01	0.156	44
$15_{9,7}-14_{6,8}$ EE	335 913.15	96	−3.8800	3.03e-02	0.049	14
$20_{13,8}-19_{12,7}$ AE	335 925.12	172	−3.3067	3.07e-02	0.013	4
$17_{16,2}-16_{15,1}$ AE	336 425.06	142	−2.8089	3.46e-02	0.137	38
$17_{16,1}-16_{15,2}$ AE	336 425.21	142	−2.8089	1.04e-01	0.137	38
$17_{16,2}-16_{15,2}$ EA	336 499.84	142	−2.8087	6.93e-02	0.116	32
$23_{13,10}-22_{14,9}$ EE	336 595.46	222	−3.3730	5.35e-02	0.043	12
$17_{16,1}-16_{15,1}$ EE	336 627.03	142	−2.8079	2.77e-01	0.267	75
$20_{13,8}-19_{12,7}$ AA	336 659.82	172	−3.3026	5.14e-02	0.019	5
$17_{16,2}-16_{15,2}$ EE	336 700.98	142	−2.8077	2.77e-01	0.220	61
$24_{11,13}-23_{12,12}$ EE	336 848.82	230	−3.0930	9.95e-02	0.105	29
$24_{12,13}-23_{11,12}$ EA	336 881.18	230	−3.0924	2.49e-02	0.036	10
$24_{12,13}-23_{11,12}$ AE	336 882.02	230	−3.0924	3.73e-02	0.036	10
$17_{16,2}-16_{15,1}$ AA	336 902.73	142	−2.8067	1.04e-01	0.224	62
$17_{16,1}-16_{15,2}$ AA	336 902.88	142	−2.8067	1.74e-01	0.224	62
$24_{11,13}-23_{12,12}$ AA	336 942.18	230	−3.0931	3.73e-02	0.053	15
$33_{1,32}-32_{2,31}$ EA	336 947.69	285	−2.7496	4.84e-02	0.158	44
$33_{2,32}-32_{1,31}$ EA	336 947.69	285	−2.7496	4.84e-02	0.158	44
$33_{2,32}-32_{2,31}$ AE	336 947.69	285	−2.7496	7.26e-02	0.158	44
$33_{1,32}-32_{1,31}$ AE	336 947.69	285	−2.7496	2.42e-02	0.158	44
$33_{1,32}-32_{2,31}$ EE	336 968.39	285	−2.8961	1.29e-01	0.221	62
$33_{2,32}-32_{2,31}$ EE	336 968.39	285	−3.1937	6.50e-02	0.221	62
$33_{1,32}-32_{1,31}$ EE	336 968.39	285	−3.1937	6.50e-02	0.221	62
$33_{2,32}-32_{1,31}$ EE	336 968.39	285	−2.8961	1.29e-01	0.221	62
$24_{12,13}-23_{11,12}$ EE	336 976.82	230	−3.0925	9.95e-02	0.129	36
$33_{1,32}-32_{2,31}$ AA	336 989.07	285	−2.7495	1.21e-01	0.187	52
$33_{2,32}-32_{1,31}$ AA	336 989.07	285	−2.7495	7.27e-02	0.187	52
$24_{12,13}-23_{11,12}$ AA	337 071.78	230	−3.0924	6.22e-02	0.084	23
$25_{10,15}-24_{11,14}$ EA	337 243.77	241	−3.0202	2.80e-02	0.059	16
$25_{10,15}-24_{11,14}$ AE	337 243.93	241	−3.0202	4.20e-02	0.087	24
$25_{11,15}-24_{10,14}$ EA	337 245.60	241	−3.0202	2.80e-02	0.045	12
$25_{11,15}-24_{10,14}$ AE	337 245.77	241	−3.0203	1.40e-02	0.045	12
$25_{10,15}-24_{11,14}$ EE	337 325.28	241	−3.0202	1.12e-01	0.060	17
$25_{11,15}-24_{10,14}$ EE	337 327.12	241	−3.0202	1.12e-01	0.060	17
$25_{10,15}-24_{11,14}$ AA	337 406.52	241	−3.0201	7.00e-02	0.038	11
$25_{11,15}-24_{10,14}$ AA	337 408.37	241	−3.0201	4.20e-02	0.038	11
$26_{9,17}-25_{10,16}$ EA	338 044.46	251	−2.9640	3.05e-02	0.168	47
$26_{10,17}-25_{9,16}$ EA	338 044.48	251	−2.9640	3.05e-02	0.168	47
$26_{9,17}-25_{10,16}$ AE	338 044.57	251	−2.9640	1.52e-02	0.168	47
$26_{10,17}-25_{9,16}$ AE	338 044.58	251	−2.9640	4.57e-02	0.168	47
$34_{0,34}-33_{1,33}$ EE	338 105.31	288	−3.4554	3.46e-02	0.243	68
$34_{1,34}-33_{1,33}$ EE	338 105.31	288	−2.7657	1.69e-01	0.243	68
$34_{0,34}-33_{0,33}$ EE	338 105.31	288	−2.7657	1.69e-01	0.243	68
$34_{1,34}-33_{0,33}$ EE	338 105.31	288	−3.4554	3.46e-02	0.243	68

Table B.1. continued.

Transition	Frequency [MHz]	$E_{\rm up}$ [K]	$\log_{10}(A_{\rm ul})$ [s^{-1}]	τ	$\int_{FWHM} I\,\delta v$ [J beam^{-1} km s^{-1}]	Detection level
$34_{0,34}-33_{0,33}$ AA	338 110.81	287	–2.7284	1.27e-01	0.197	55
$34_{1,34}-33_{1,33}$ AA	338 110.81	287	–2.7283	7.65e-02	0.197	55
$26_{9,17}-25_{10,16}$ EE	338 117.64	251	–2.9640	1.22e-01	0.210	59
$26_{10,17}-25_{9,16}$ EE	338 117.66	251	–2.9640	1.22e-01	0.210	59
$26_{9,17}-25_{10,16}$ AA	338 190.61	251	–2.9638	4.57e-02	0.114	32
$26_{10,17}-25_{9,16}$ AA	338 190.62	251	–2.9638	7.61e-02	0.114	32
$18_{14,5}-17_{13,5}$ EA	338 648.66	147	–3.0058	4.43e-02	0.030	8
$18_{14,4}-17_{13,4}$ EE	338 833.86	147	–3.0148	1.73e-01	0.148	41
$18_{14,4}-17_{13,5}$ AE	339 030.13	147	–2.9994	2.24e-02	0.018	5
$27_{8,19}-26_{9,18}$ EE	339 069.60	260	–2.9174	1.30e-01	0.173	48
$27_{9,19}-26_{8,18}$ EE	339 069.60	260	–2.9174	1.30e-01	0.173	48
$27_{8,19}-26_{9,18}$ AA	339 136.45	260	–2.9173	8.13e-02	0.119	33
$27_{9,19}-26_{8,18}$ AA	339 136.45	260	–2.9172	4.88e-02	0.119	33
$14_{5,9}-13_{4,10}$ EE	339 242.67	76	–4.2327	1.44e-02	0.032	9
$23_{13,11}-22_{12,10}$ EE	339 955.49	219	–3.1917	8.21e-02	0.078	22
$28_{7,21}-27_{8,20}$ EA	340 038.58	269	–2.8776	3.44e-02	0.136	38
$28_{8,21}-27_{7,20}$ EA	340 038.58	269	–2.8776	3.44e-02	0.136	38
$28_{7,21}-27_{8,20}$ AE	340 038.65	269	–2.8777	1.72e-02	0.136	38
$28_{8,21}-27_{7,20}$ AE	340 038.65	269	–2.8776	5.16e-02	0.136	38
$28_{7,21}-27_{8,20}$ EE	340 100.55	269	–2.8776	1.37e-01	0.187	52
$28_{8,21}-27_{7,20}$ EE	340 100.55	269	–2.8776	1.37e-01	0.187	52
$28_{7,21}-27_{8,20}$ AA	340 162.36	269	–2.8774	5.16e-02	0.112	31
$28_{8,21}-27_{7,20}$ AA	340 162.36	269	–2.8774	8.59e-02	0.112	31
$29_{7,23}-28_{7,22}$ EA	341 116.83	276	–2.8426	3.61e-02	0.132	37
$29_{6,23}-28_{6,22}$ EA	341 116.83	276	–2.8426	3.61e-02	0.132	37
$29_{6,23}-28_{6,22}$ AE	341 116.89	276	–2.8426	1.81e-02	0.132	37
$29_{7,23}-28_{7,22}$ AE	341 116.89	276	–2.8426	5.42e-02	0.132	37
$29_{7,23}-28_{7,22}$ EE	341 174.15	276	–6.0035	9.97e-05	0.200	56
$29_{6,23}-28_{7,22}$ EE	341 174.15	276	–2.8428	1.44e-01	0.200	56
$29_{6,23}-28_{6,22}$ EE	341 174.15	276	–6.0035	9.97e-05	0.200	56
$29_{7,23}-28_{6,22}$ EE	341 174.15	276	–2.8428	1.44e-01	0.200	56
$29_{6,23}-28_{7,22}$ AA	341 231.36	276	–2.8423	9.03e-02	0.132	37
$29_{7,23}-28_{6,22}$ AA	341 231.36	276	–2.8424	5.42e-02	0.132	37
$44_{5,39}-44_{5,40}$ EE	341 950.48	562	–3.5251	3.21e-03	0.013	4
$44_{6,39}-44_{5,40}$ EE	341 950.48	562	–4.1489	7.62e-04	0.013	4
$44_{5,39}-44_{4,40}$ EE	341 950.48	562	–4.1489	7.62e-04	0.013	4
$44_{6,39}-44_{4,40}$ EE	341 950.48	562	–3.5251	3.21e-03	0.013	4
$30_{6,25}-29_{6,24}$ EA	342 219.92	283	–2.8113	3.78e-02	0.124	35
$30_{5,25}-29_{5,24}$ EA	342 219.92	283	–2.8113	3.78e-02	0.124	35
$30_{5,25}-29_{5,24}$ AE	342 219.97	283	–2.8113	5.67e-02	0.124	35
$30_{6,25}-29_{6,24}$ AE	342 219.97	283	–2.8113	1.89e-02	0.124	35
$30_{5,25}-29_{6,24}$ EE	342 272.48	283	–3.8339	1.43e-02	0.208	58
$30_{6,25}-29_{6,24}$ EE	342 272.48	283	–2.8544	1.37e-01	0.208	58
$30_{5,25}-29_{5,24}$ EE	342 272.48	283	–2.8544	1.37e-01	0.208	58
$30_{6,25}-29_{5,24}$ EE	342 272.48	283	–3.8339	1.43e-02	0.208	58
$17_{17,1}-16_{16,0}$ AE	342 300.57	147	–2.7347	3.83e-02	0.142	40
$17_{17,0}-16_{16,1}$ AE	342 300.57	147	–2.7346	1.15e-01	0.142	40
$30_{5,25}-29_{6,24}$ AA	342 324.94	283	–2.8110	5.67e-02	0.130	36
$30_{6,25}-29_{5,24}$ AA	342 324.94	283	–2.8111	9.45e-02	0.130	36
$17_{17,1}-16_{16,1}$ EA	342 410.64	147	–2.7343	7.67e-02	0.095	26
$17_{17,0}-16_{16,0}$ EE	342 485.23	147	–2.7339	3.06e-01	0.269	75
$17_{17,1}-16_{16,1}$ EE	342 594.89	147	–2.7335	3.07e-01	0.229	64
$17_{17,1}-16_{16,0}$ AA	342 780.03	147	–2.7327	1.15e-01	0.227	63
$17_{17,0}-16_{16,1}$ AA	342 780.04	147	–2.7328	1.92e-01	0.227	63
$31_{4,27}-30_{5,26}$ EA	343 338.88	289	–2.7830	3.95e-02	0.142	40
$31_{5,27}-30_{4,26}$ EA	343 338.88	289	–2.7830	3.95e-02	0.142	40
$31_{4,27}-30_{4,26}$ AE	343 338.92	289	–2.7830	1.97e-02	0.142	40
$31_{5,27}-30_{5,26}$ AE	343 338.92	289	–2.7830	5.92e-02	0.142	40
$31_{4,27}-30_{5,26}$ AA	343 433.08	289	–2.7828	9.87e-02	0.172	48
$31_{5,27}-30_{4,26}$ AA	343 433.08	289	–2.7828	5.92e-02	0.172	48

Table B.1. continued.

Transition	Frequency [MHz]	$E_{\rm up}$ [K]	$\log_{10}(A_{\rm ul})$ [s^{-1}]	τ	$\int_{FWHM} I\,\delta v$ [J beam^{-1} km s^{-1}]	Detection level
$32_{3,29}-31_{4,28}$ EA	344 468.95	294	−2.7572	4.12e-02	0.114	32
$32_{4,29}-31_{3,28}$ EA	344 468.95	294	−2.7572	4.12e-02	0.114	32
$32_{4,29}-31_{4,28}$ AE	344 468.98	294	−2.7572	2.06e-02	0.114	32
$32_{3,29}-31_{3,28}$ AE	344 468.98	294	−2.7572	6.19e-02	0.114	32
$32_{3,29}-31_{3,28}$ EE	344 509.42	294	−3.7739	1.52e-02	0.182	51
$32_{3,29}-31_{4,28}$ EE	344 509.42	294	−2.7817	1.50e-01	0.182	51
$32_{4,29}-31_{3,28}$ EE	344 509.42	294	−2.7817	1.50e-01	0.182	51
$32_{4,29}-31_{4,28}$ EE	344 509.42	294	−3.7739	1.52e-02	0.182	51
$32_{3,29}-31_{4,28}$ AA	344 549.87	294	−2.7569	6.19e-02	0.181	51
$32_{4,29}-31_{3,28}$ AA	344 549.87	294	−2.7570	1.03e-01	0.181	51
$18_{15,3}-17_{14,3}$ EE	345 037.50	151	−2.8914	2.16e-01	0.142	40
$18_{15,4}-17_{14,4}$ EE	345 073.72	151	−2.8917	2.15e-01	0.210	59
$33_{3,31}-32_{3,30}$ EA	345 607.71	298	−2.7333	4.31e-02	0.183	51
$33_{2,31}-32_{2,30}$ EA	345 607.71	298	−2.7333	4.31e-02	0.183	51
$33_{3,31}-32_{3,30}$ AE	345 607.74	298	−2.7334	6.46e-02	0.183	51
$33_{2,31}-32_{2,30}$ AE	345 607.74	298	−2.7334	2.15e-02	0.183	51
$33_{2,31}-32_{3,30}$ EE	345 639.62	298	−3.5454	2.48e-02	0.200	56
$33_{2,31}-32_{2,30}$ EE	345 639.62	298	−2.7700	1.48e-01	0.200	56
$33_{3,31}-32_{3,30}$ EE	345 639.62	298	−2.7700	1.48e-01	0.200	56
$33_{3,31}-32_{2,30}$ EE	345 639.62	298	−3.5454	2.48e-02	0.200	56
$33_{2,31}-32_{2,30}$ AA	345 671.52	298	−2.7332	6.47e-02	0.140	39
$33_{3,31}-32_{3,30}$ AA	345 671.52	298	−2.7332	1.08e-01	0.140	39
$25_{11,14}-24_{12,13}$ EA	346 346.12	247	−3.0311	2.48e-02	0.078	22
$25_{11,14}-24_{12,13}$ AE	346 346.31	247	−3.0310	3.72e-02	0.078	22
$25_{12,14}-24_{11,13}$ EA	346 374.84	247	−3.0309	2.48e-02	0.042	12
$25_{12,14}-24_{11,13}$ AE	346 375.23	247	−3.0310	1.24e-02	0.042	12
$25_{11,14}-24_{12,13}$ EE	346 432.88	247	−3.0311	9.90e-02	0.091	25
$25_{12,14}-24_{11,13}$ EE	346 461.91	247	−3.0310	9.90e-02	0.068	19
$25_{11,14}-24_{12,13}$ AA	346 519.31	247	−3.0311	6.19e-02	0.042	12
$25_{12,14}-24_{11,13}$ AA	346 548.56	247	−3.0309	3.71e-02	0.067	19
$34_{1,33}-33_{2,32}$ AA	346 795.27	301	−2.7111	6.78e-02	0.097	27
$34_{2,33}-33_{1,32}$ AA	346 795.27	301	−2.7112	1.13e-01	0.097	27
$26_{10,16}-25_{11,15}$ EA	346 941.16	258	−2.9664	2.73e-02	0.081	23
$26_{10,16}-25_{11,15}$ AE	346 941.30	258	−2.9664	1.37e-02	0.081	23
$26_{11,16}-25_{10,15}$ EA	346 941.51	258	−2.9664	2.73e-02	0.081	23
$26_{11,16}-25_{10,15}$ AE	346 941.65	258	−2.9664	4.09e-02	0.081	23
$26_{10,16}-25_{11,15}$ EE	347 017.52	258	−2.9663	1.09e-01	0.142	40
$26_{11,16}-25_{10,15}$ EE	347 017.87	258	−2.9663	1.09e-01	0.142	40
$26_{10,16}-25_{11,15}$ AA	347 093.62	258	−2.9662	4.09e-02	0.101	28
$26_{11,16}-25_{10,15}$ AA	347 093.97	258	−2.9663	6.82e-02	0.101	28
$24_{13,12}-23_{12,11}$ EE	347 309.14	235	−3.1182	8.51e-02	0.099	28
$27_{9,18}-26_{10,17}$ EA	347 797.75	268	−2.9148	2.93e-02	0.138	39
$27_{10,18}-26_{9,17}$ EA	347 797.75	268	−2.9148	2.93e-02	0.138	39
$27_{9,18}-26_{10,17}$ AE	347 797.85	268	−2.9148	4.40e-02	0.138	39
$27_{10,18}-26_{9,17}$ AE	347 797.85	268	−2.9148	1.47e-02	0.138	39
$27_{9,18}-26_{10,17}$ EE	347 867.07	268	−2.9147	1.17e-01	0.186	52
$27_{10,18}-26_{9,17}$ EE	347 867.08	268	−2.9147	1.17e-01	0.186	52
$35_{0,35}-34_{1,34}$ AE	347 907.80	304	−2.6907	7.10e-02	0.130	36
$35_{1,35}-34_{0,34}$ AE	347 907.80	304	−2.6907	2.37e-02	0.130	36
$35_{0,35}-34_{1,34}$ EA	347 907.85	304	−2.6907	4.73e-02	0.130	36
$35_{1,35}-34_{0,34}$ EA	347 907.85	304	−2.6907	4.73e-02	0.130	36
$35_{0,35}-34_{1,34}$ AA	347 918.78	304	−2.6907	1.18e-01	0.133	37
$35_{1,35}-34_{0,34}$ AA	347 918.78	304	−2.6907	7.11e-02	0.133	37
$27_{9,18}-26_{10,17}$ AA	347 936.19	268	−2.9146	7.33e-02	0.085	24
$27_{10,18}-26_{9,17}$ AA	347 936.20	268	−2.9145	4.40e-02	0.085	24
$28_{8,20}-27_{9,19}$ EA	348 780.22	277	−2.8714	3.10e-02	0.092	26
$28_{9,20}-27_{8,19}$ EA	348 780.22	277	−2.8714	3.10e-02	0.092	26
$28_{8,20}-27_{9,19}$ AE	348 780.29	277	−2.8713	1.55e-02	0.092	26
$28_{9,20}-27_{8,19}$ AE	348 780.29	277	−2.8714	4.65e-02	0.092	26
$28_{8,20}-27_{9,19}$ EE	348 844.27	277	−2.8712	1.24e-01	0.144	40

Table B.1. continued.

Transition	Frequency [MHz]	$E_{\rm up}$ [K]	$\log_{10}(A_{\rm ul})$ [s^{-1}]	τ	$\int_{FWHM} I\,\delta v$ [J beam^{-1} km s^{-1}]	Detection level
$28_{9,20}-27_{8,19}$ EE	348 844.27	277	−2.8712	1.24e-01	0.144	40
$28_{8,20}-27_{9,19}$ AA	348 908.15	277	−2.8711	4.65e-02	0.097	27
$28_{9,20}-27_{8,19}$ AA	348 908.15	277	−2.8711	7.76e-02	0.097	27
$14_{4,10}-13_{3,11}$ EE	348 964.09	72	−4.4168	9.23e-03	0.014	4
$14_{5,10}-13_{2,11}$ EE	348 964.42	72	−4.4168	9.23e-03	0.014	4
$29_{7,22}-28_{8,21}$ EA	349 827.76	285	−2.8337	3.26e-02	0.120	34
$29_{8,22}-28_{7,21}$ EA	349 827.76	285	−2.8337	3.26e-02	0.120	34
$29_{7,22}-28_{8,21}$ AE	349 827.82	285	−2.8338	4.89e-02	0.120	34
$29_{8,22}-28_{7,21}$ AE	349 827.82	285	−2.8338	1.63e-02	0.120	34
$29_{8,22}-28_{8,21}$ EE	349 887.43	285	−2.8633	1.22e-01	0.150	42
$29_{7,22}-28_{8,21}$ EE	349 887.43	285	−4.0142	8.60e-03	0.150	42
$29_{7,22}-28_{7,21}$ EE	349 887.43	285	−2.8631	1.22e-01	0.150	42
$29_{8,22}-28_{7,21}$ EE	349 887.43	285	−4.0172	8.54e-03	0.150	42
$29_{7,22}-28_{8,21}$ AA	349 946.96	285	−2.8335	8.14e-02	0.100	28
$29_{8,22}-28_{7,21}$ AA	349 946.96	285	−2.8334	4.89e-02	0.100	28
$18_{16,3}-17_{15,2}$ AE	350 819.12	155	−2.8044	9.25e-02	0.070	19
$18_{16,2}-17_{15,3}$ AE	350 821.27	155	−2.8044	3.08e-02	0.015	4
$18_{16,3}-17_{15,3}$ EA	350 891.89	155	−2.8043	6.17e-02	0.047	13
$30_{6,24}-29_{6,23}$ EA	350 911.96	293	−2.8004	3.40e-02	0.118	33
$30_{7,24}-29_{7,23}$ EA	350 911.96	293	−2.8004	3.40e-02	0.118	33
$30_{6,24}-29_{6,23}$ AE	350 912.01	293	−2.8004	5.10e-02	0.118	33
$30_{7,24}-29_{7,23}$ AE	350 912.01	293	−2.8004	1.70e-02	0.118	33
$30_{6,24}-29_{6,23}$ EE	350 967.54	293	−3.4934	2.76e-02	0.187	52
$30_{6,24}-29_{7,23}$ EE	350 967.54	293	−2.8987	1.09e-01	0.187	52
$30_{7,24}-29_{7,23}$ EE	350 967.54	293	−3.2594	4.73e-02	0.187	52
$30_{7,24}-29_{6,23}$ EE	350 967.54	293	−2.9856	8.88e-02	0.187	52
$18_{16,2}-17_{15,2}$ EE	351 012.48	155	−2.8033	2.47e-01	0.214	60
$30_{7,24}-29_{7,23}$ AA	351 023.02	293	−2.8002	5.10e-02	0.111	31
$30_{6,24}-29_{6,23}$ AA	351 023.02	293	−2.8002	8.51e-02	0.111	31
$18_{16,3}-17_{15,3}$ EE	351 083.30	155	−2.8032	2.47e-01	0.182	51
$18_{16,3}-17_{15,2}$ AA	351 274.14	155	−2.8021	1.55e-01	0.115	32
$31_{5,26}-30_{5,25}$ EA	352 018.43	300	−2.7706	3.55e-02	0.135	38
$31_{6,26}-30_{6,25}$ EA	352 018.43	300	−2.7706	3.55e-02	0.135	38
$31_{5,26}-30_{6,25}$ AE	352 018.48	300	−2.7706	5.32e-02	0.135	38
$31_{6,26}-30_{5,25}$ AE	352 018.48	300	−2.7705	1.77e-02	0.135	38
$31_{5,26}-30_{6,25}$ EE	352 069.73	300	−5.6440	1.88e-04	0.187	52
$31_{5,26}-30_{5,25}$ EE	352 069.73	300	−2.7671	1.42e-01	0.187	52
$31_{6,26}-30_{6,25}$ EE	352 069.73	300	−2.7671	1.42e-01	0.187	52
$31_{6,26}-30_{5,25}$ EE	352 069.73	300	−5.6440	1.88e-04	0.187	52
$31_{5,26}-30_{5,25}$ AA	352 120.94	300	−2.7703	5.32e-02	0.136	38
$31_{6,26}-30_{6,25}$ AA	352 120.94	300	−2.7703	8.87e-02	0.136	38
$24_{13,11}-23_{14,10}$ EE	352 593.82	239	−3.2028	6.58e-02	0.080	22
$19_{14,6}-18_{13,6}$ EA	352 777.63	161	−3.1271	2.93e-02	0.033	9
$16_{11,6}-15_{8,7}$ EE	352 842.59	113	−3.8606	2.68e-02	0.035	10
$16_{11,6}-15_{8,7}$ EE	352 842.59	113	−3.8606	2.68e-02	0.029	8
$32_{4,28}-31_{5,27}$ EA	353 139.60	306	−2.7434	3.69e-02	0.116	32
$32_{5,28}-31_{4,27}$ EA	353 139.60	306	−2.7434	3.69e-02	0.116	32
$32_{4,28}-31_{4,27}$ AE	353 139.65	306	−2.7434	5.54e-02	0.116	32
$32_{5,28}-31_{5,27}$ AE	353 139.65	306	−2.7433	1.85e-02	0.116	32
$32_{4,28}-31_{4,27}$ EE	353 185.88	306	−2.7258	1.48e-01	0.185	52
$32_{5,28}-31_{5,27}$ EE	353 185.88	306	−2.7258	1.48e-01	0.185	52
$32_{4,28}-31_{5,27}$ AA	353 232.11	306	−2.7431	5.54e-02	0.114	32
$32_{5,28}-31_{4,27}$ AA	353 232.11	306	−2.7432	9.23e-02	0.114	32
$16_{10,7}-15_{7,8}$ EE	353 644.50	110	−3.7796	3.29e-02	0.061	17
$16_{10,7}-15_{7,8}$ AA	353 896.48	110	−3.7790	2.06e-02	0.033	9
$33_{3,30}-32_{4,29}$ EA	354 271.40	311	−2.7185	3.84e-02	0.171	48
$33_{4,30}-32_{3,29}$ EA	354 271.40	311	−2.7185	3.84e-02	0.171	48
$33_{3,30}-32_{3,29}$ AE	354 271.44	311	−2.7185	1.92e-02	0.171	48
$33_{4,30}-32_{4,29}$ AE	354 271.44	311	−2.7185	5.76e-02	0.171	48
$19_{14,5}-18_{13,6}$ AE	354 307.91	161	−3.0237	5.52e-02	0.033	9

Table B.1. continued.

Transition	Frequency [MHz]	$E_{\rm up}$ [K]	$\log_{10}(A_{\rm ul})$ [s^{-1}]	τ	$\int_{FWHM} I\,\delta v$ [J beam^{-1} km s^{-1}]	Detection level
$33_{3,30}-32_{4,29}$ EE	354 311.36	311	−3.6682	1.61e-02	0.269	75
$33_{3,30}-32_{3,29}$ EE	354 311.36	311	−2.7358	1.38e-01	0.269	75
$33_{4,30}-32_{4,29}$ EE	354 311.36	311	−2.7358	1.38e-01	0.269	75
$33_{4,30}-32_{3,29}$ EE	354 311.36	311	−3.6682	1.61e-02	0.269	75
$33_{3,30}-32_{4,29}$ AA	354 351.30	311	−2.7183	9.61e-02	0.176	49
$33_{4,30}-32_{3,29}$ AA	354 351.30	311	−2.7183	5.77e-02	0.176	49
$34_{2,32}-33_{3,31}$ EA	355 411.74	315	−2.6955	4.00e-02	0.129	36
$34_{3,32}-33_{2,31}$ EA	355 411.74	315	−2.6955	4.00e-02	0.129	36
$34_{2,32}-33_{2,31}$ AE	355 411.77	315	−2.6955	6.00e-02	0.129	36
$34_{3,32}-33_{3,31}$ AE	355 411.77	315	−2.6955	2.00e-02	0.129	36
$34_{3,32}-33_{3,31}$ EE	355 443.39	315	−2.6521	1.60e-01	0.201	56
$34_{2,32}-33_{2,31}$ EE	355 443.39	315	−2.6521	1.60e-01	0.201	56
$34_{3,32}-33_{3,31}$ AA	355 475.05	315	−2.6953	6.01e-02	0.239	67
$34_{2,32}-33_{2,31}$ AA	355 475.05	315	−2.6953	1.00e-01	0.239	67
$25_{12,13}-24_{13,12}$ AE	355 620.72	252	−3.0519	3.23e-02	0.053	15
$25_{12,13}-24_{13,12}$ EA	355 621.08	252	−3.0519	2.15e-02	0.053	15
$25_{12,13}-24_{13,12}$ EE	355 713.67	252	−3.0520	8.60e-02	0.092	26
$25_{12,13}-24_{13,12}$ AA	355 806.17	252	−3.0520	5.37e-02	0.040	11
$26_{12,15}-25_{11,14}$ EA	355 972.75	264	−2.9740	2.43e-02	0.064	18
$26_{12,15}-25_{11,14}$ AE	355 972.99	264	−2.9740	3.64e-02	0.064	18
$26_{11,15}-25_{12,14}$ EE	356 046.79	264	−2.9739	9.71e-02	0.110	31
$26_{12,15}-25_{11,14}$ EE	356 052.97	264	−2.9739	9.71e-02	0.107	30
$25_{13,13}-24_{12,12}$ EE	356 066.12	252	−3.0504	8.61e-02	0.124	35
$26_{12,15}-25_{11,14}$ AA	356 132.86	264	−2.9739	6.07e-02	0.057	16
$35_{1,34}-34_{1,33}$ EA	356 559.73	319	−2.6741	4.18e-02	0.127	35
$35_{2,34}-34_{2,33}$ EA	356 559.73	319	−2.6741	4.18e-02	0.127	35
$35_{1,34}-34_{1,33}$ AE	356 559.73	319	−2.6741	2.09e-02	0.127	35
$35_{2,34}-34_{2,33}$ AE	356 559.73	319	−2.6740	6.27e-02	0.127	35
$35_{1,34}-34_{2,33}$ EE	356 580.23	319	−2.6206	1.66e-01	0.196	55
$35_{2,34}-34_{2,33}$ EE	356 580.23	319	−4.8932	8.88e-04	0.196	55
$35_{1,34}-34_{1,33}$ EE	356 580.23	319	−4.8932	8.88e-04	0.196	55
$35_{2,34}-34_{1,33}$ EE	356 580.23	319	−2.6206	1.66e-01	0.196	55
$35_{1,34}-34_{2,33}$ AA	356 600.73	319	−2.6740	1.05e-01	0.128	36
$35_{2,34}-34_{1,33}$ AA	356 600.73	319	−2.6740	6.28e-02	0.128	36
$18_{17,1}-17_{16,1}$ EA	356 621.39	160	−2.7275	6.88e-02	0.065	18
$27_{10,17}-26_{11,16}$ EA	356 658.41	275	−2.9156	2.63e-02	0.112	31
$27_{11,17}-26_{10,16}$ EA	356 658.48	275	−2.9156	2.63e-02	0.112	31
$27_{10,17}-26_{11,16}$ AE	356 658.54	275	−2.9156	3.95e-02	0.112	31
$27_{11,17}-26_{10,16}$ AE	356 658.60	275	−2.9156	1.32e-02	0.112	31
$18_{17,2}-17_{16,1}$ AE	356 727.49	159	−2.7272	1.03e-01	0.070	20
$18_{17,1}-17_{16,2}$ AE	356 727.54	159	−2.7272	3.44e-02	0.070	20
$27_{10,17}-26_{11,16}$ AA	356 801.31	275	−2.9153	6.58e-02	0.097	27
$27_{11,17}-26_{10,16}$ AA	356 801.37	275	−2.9154	3.95e-02	0.097	27
$18_{17,2}-17_{16,2}$ EA	356 833.46	159	−2.7269	6.89e-02	0.078	22
$18_{17,1}-17_{16,1}$ EE	356 902.77	160	−2.7263	2.75e-01	0.193	54
$18_{17,2}-17_{16,2}$ EE	357 008.08	159	−2.7261	2.76e-01	0.289	81
$18_{17,2}-17_{16,1}$ AA	357 183.43	160	−2.7252	1.72e-01	0.225	63
$18_{17,1}-17_{16,2}$ AA	357 183.48	160	−2.7253	1.03e-01	0.225	63
$28_{9,19}-27_{10,18}$ EA	357 558.00	285	−2.8678	2.80e-02	0.106	30
$28_{10,19}-27_{9,18}$ EA	357 558.01	285	−2.8678	2.80e-02	0.106	30
$28_{9,19}-27_{10,18}$ AE	357 558.09	285	−2.8678	1.40e-02	0.106	30
$28_{10,19}-27_{9,18}$ AE	357 558.09	285	−2.8678	4.20e-02	0.106	30
$28_{9,19}-27_{10,18}$ EE	357 623.66	285	−2.8677	1.12e-01	0.182	51
$28_{10,19}-27_{9,18}$ EE	357 623.66	285	−2.8677	1.12e-01	0.182	51
$28_{9,19}-27_{10,18}$ AA	357 689.11	285	−2.8675	4.20e-02	0.127	35
$28_{10,19}-27_{9,18}$ AA	357 689.11	285	−2.8676	6.99e-02	0.127	35
$36_{0,36}-35_{0,35}$ AE	357 715.22	322	−2.6541	6.56e-02	0.154	43
$36_{1,36}-35_{1,35}$ AE	357 715.22	322	−2.6541	2.19e-02	0.154	43
$36_{0,36}-35_{1,35}$ EA	357 715.27	322	−2.6541	4.37e-02	0.154	43
$36_{1,36}-35_{0,35}$ EA	357 715.27	322	−2.6541	4.37e-02	0.154	43

Table B.1. continued.

Transition	Frequency [MHz]	$E_{\rm up}$ [K]	$\log_{10}(A_{\rm ul})$ [s^{-1}]	τ	$\int_{FWHM} I\,\delta v$ [J beam^{-1} km s^{-1}]	Detection level
$36_{0,36}-35_{1,35}$ EE	357 720.70	321	−2.5866	1.75e-01	0.235	66
$36_{1,36}-35_{1,35}$ EE	357 720.70	321	−5.6153	1.64e-04	0.235	66
$36_{1,36}-35_{0,35}$ EE	357 720.70	321	−2.5866	1.75e-01	0.235	66
$36_{0,36}-35_{0,35}$ EE	357 720.70	321	−5.6153	1.64e-04	0.235	66
$36_{0,36}-35_{1,35}$ AA	357 726.06	321	−2.6541	6.57e-02	0.155	43
$36_{1,36}-35_{0,35}$ AA	357 726.06	321	−2.6541	1.09e-01	0.155	43
$29_{8,21}-28_{9,20}$ EA	358 560.03	294	−2.8271	2.94e-02	0.126	35
$29_{9,21}-28_{8,20}$ EA	358 560.03	294	−2.8271	2.94e-02	0.126	35
$29_{8,21}-28_{9,20}$ AE	358 560.10	294	−2.8271	4.41e-02	0.126	35
$29_{9,21}-28_{8,20}$ AE	358 560.10	294	−2.8270	1.47e-02	0.126	35
$29_{8,21}-28_{9,20}$ EE	358 621.21	294	−2.8269	1.18e-01	0.195	55
$29_{9,21}-28_{8,20}$ EE	358 621.21	294	−2.8269	1.18e-01	0.195	55
$29_{8,21}-28_{9,20}$ AA	358 682.23	294	−2.8268	7.34e-02	0.118	33
$29_{9,21}-28_{8,20}$ AA	358 682.23	294	−2.8268	4.41e-02	0.118	33
$19_{15,5}-18_{14,5}$ EA	359 063.67	164	−2.9024	4.61e-02	0.052	15
$19_{15,4}-18_{14,4}$ EE	359 225.22	164	−2.9025	1.84e-01	0.159	44
$19_{15,5}-18_{14,5}$ EE	359 266.93	164	−2.9031	1.84e-01	0.142	40
$30_{8,23}-29_{8,22}$ EA	359 617.24	303	−2.7914	3.07e-02	0.119	33
$30_{7,23}-29_{7,22}$ EA	359 617.24	303	−2.7914	3.07e-02	0.119	33
$30_{7,23}-29_{8,22}$ AE	359 617.31	303	−2.7914	1.53e-02	0.119	33
$30_{8,23}-29_{7,22}$ AE	359 617.31	303	−2.7914	4.60e-02	0.119	33
$30_{7,23}-29_{8,22}$ EE	359 674.69	303	−4.9449	8.61e-04	0.163	45
$30_{8,23}-29_{8,22}$ EE	359 674.69	303	−2.7943	1.22e-01	0.163	45
$30_{8,23}-29_{7,22}$ EE	359 674.69	303	−4.9449	8.61e-04	0.163	45
$30_{7,23}-29_{7,22}$ EE	359 674.69	303	−2.7943	1.22e-01	0.163	45
$30_{8,23}-29_{8,22}$ AA	359 731.98	303	−2.7912	4.60e-02	0.100	28
$30_{8,23}-29_{8,22}$ AA	359 731.98	303	−2.7912	4.60e-02	0.102	28
$30_{7,23}-29_{7,22}$ AA	359 731.98	303	−2.7911	7.67e-02	0.100	28
$30_{7,23}-29_{7,22}$ AA	359 731.98	303	−2.7911	7.67e-02	0.102	28
$31_{6,25}-30_{7,24}$ EA	360 706.63	310	−2.7597	3.19e-02	0.152	42
$31_{7,25}-30_{6,24}$ EA	360 706.63	310	−2.7597	3.19e-02	0.152	42
$31_{6,25}-30_{7,24}$ AE	360 706.68	310	−2.7597	4.78e-02	0.152	42
$31_{7,25}-30_{6,24}$ AE	360 706.68	310	−2.7597	1.59e-02	0.152	42
$31_{7,25}-30_{7,24}$ EE	360 760.53	310	−2.7647	1.25e-01	0.175	49
$31_{6,25}-30_{7,24}$ EE	360 760.53	310	−4.4450	2.61e-03	0.175	49
$31_{6,25}-30_{6,24}$ EE	360 760.53	310	−2.7559	1.27e-01	0.175	49
$31_{7,25}-30_{6,24}$ EE	360 760.53	310	−6.1629	4.99e-05	0.175	49
$31_{6,25}-30_{6,24}$ AA	360 814.30	310	−2.7595	4.78e-02	0.097	27
$31_{7,25}-30_{7,24}$ AA	360 814.30	310	−2.7594	7.97e-02	0.097	27
$23_{14,10}-22_{13,9}$ EE	360 915.54	223	−3.2141	6.73e-02	0.088	25
$32_{6,27}-31_{6,26}$ EA	361 816.20	317	−2.7310	3.31e-02	0.155	43
$32_{5,27}-31_{5,26}$ EA	361 816.20	317	−2.7310	3.31e-02	0.155	43
$32_{5,27}-31_{5,26}$ AE	361 816.25	317	−2.7310	4.96e-02	0.155	43
$32_{6,27}-31_{6,26}$ AE	361 816.25	317	−2.7311	1.65e-02	0.155	43
$32_{5,27}-31_{6,26}$ EE	361 866.27	317	−2.7219	1.30e-01	0.204	57
$32_{6,27}-31_{6,26}$ EE	361 866.27	317	−4.4333	2.52e-03	0.204	57
$32_{5,27}-31_{5,26}$ EE	361 866.27	317	−4.4333	2.52e-03	0.204	57
$32_{6,27}-31_{5,26}$ EE	361 866.27	317	−2.7219	1.30e-01	0.204	57
$32_{5,27}-31_{6,26}$ AA	361 916.24	317	−2.7308	4.96e-02	0.133	37
$32_{6,27}-31_{5,26}$ AA	361 916.24	317	−2.7308	8.27e-02	0.133	37
$24_{14,11}-23_{13,10}$ EE	362 230.43	240	−3.1534	6.99e-02	0.063	18
$18_{18,0}-17_{17,0}$ EA	362 458.25	164	−2.6580	7.52e-02	0.061	17
$18_{18,1}-17_{17,0}$ AE	362 600.03	164	−2.6576	1.13e-01	0.154	43
$18_{18,0}-17_{17,1}$ AE	362 600.03	164	−2.6576	3.76e-02	0.154	43
$18_{18,1}-17_{17,1}$	362 741.13	164	−2.6571	7.54e-02	0.173	48
$18_{18,0}-17_{17,0}$ EE	362 755.32	164	−2.6569	3.01e-01	0.239	67
$16_{9,8}-15_{6,9}$ EA	362 811.49	107	−3.8228	7.25e-03	0.019	5

Appendix C: Acetone lines with high K_a and low K_c quantum numbers

Table C.1. Acetone lines with high K_a and low K_c quantum numbers

Transition	Predicted frequency [MHz]
$19_{13,7}$–$18_{12,6}$ EE	334 948.01
$18_{13,5}$–$17_{12,6}$ EE	336 133.79
$18_{14,5}$–$17_{13,4}$ AE	338 242.61
$18_{14,4}$–$17_{13,4}$ EA	338 625.87
$18_{14,4}$–$17_{13,5}$ AA	339 459.74
$18_{12,6}$–$17_{11,7}$ EE	342 896.39
$18_{15,3}$–$17_{14,3}$ EA	344 793.57
$19_{14,6}$–$18_{13,5}$ EE	350 205.27
$19_{14,6}$–$18_{13,5}$ AA	351 215.21
$19_{14,6}$–$18_{13,6}$ EE	353 155.67
$19_{14,5}$–$18_{13,6}$ AA	354 673.02
$19_{14,5}$–$18_{13,6}$ EE	355 248.54
$19_{13,6}$–$18_{12,7}$ AA	356 644.96
$19_{13,6}$–$18_{12,7}$ EE	356 675.20
$19_{15,4}$–$18_{14,5}$ AE	359 197.90
$19_{15,5}$–$18_{14,4}$ AA	359 301.10
$20_{14,7}$–$19_{13,6}$ EE	359 843.80
$20_{14,7}$–$19_{13,6}$ AA	360 338.51

Notes. These acetone lines appear missing or shifted when comparing the synthetic spectrum with the observed spectrum. This could be due to perturbations by interactions between the (high K_a, low K_c) levels and the levels from the lowest torsional excited states (Groner et al. 2002).